Title: A connexin 43 targeting peptide prevents blood vessel neointima formation

Running Title: CycliCx peptide disrupts neointima

Authors: Meghan W. Sedovy[1,2#], Mark C. Renton[1#], Xinyan Leng[1], Farwah Iqbal[3], Melissa R. Leaf[3], Kailynn Roberts[1,2], Ramya C. Joshi[1], Arya Malek[1], Clare L. Dennison[1], Angela K Best[4], Paul D. Lampe[5], Joseph W. Baker[3,6], Mark Joseph[3,6], George S. Baillie[7], Brant E. Isakson[4,8] and Scott R. Johnstone[1,3,6,9*]

Affiliations:

[1] The Fralin Biomedical Research Institute at Virginia Tech Carilion, Center for Vascular and Heart Research, 4 Riverside Circle, Roanoke, Virginia, VA 24016 USA

[2] Translational Biology, Medicine, and Health Graduate Program, Virginia Tech, Blacksburg, VA 24061, USA

[3] Virginia Tech Carilion School of Medicine, Roanoke, VA 24016 USA

[4] Robert M. Berne Cardiovascular Research Center, University of Virginia School of Medicine, Virginia, VA 22908, USA

[5] Fred Hutchinson Cancer Research Center, Seattle, WA 98109 USA.

[6] Department of Surgery, Virginia Tech Carilion School of Medicine, Roanoke, VA 24016 USA

[7] School of Cardiovascular and Metabolic Health, University of Glasgow, Glasgow, UK G128QQ, UK

[8] Department of Molecular Physiology and Biophysics, University of Virginia School of Medicine, Virginia, VA 22908, USA

[9] Department of Biological Sciences, College of Science, Virginia Tech, Blacksburg, VA 24061, USA

Coauthors: Meghan W. Sedovy and Mark C. Renton share the position of first author.

* **Corresponding Author:**

Scott R. Johnstone, The Fralin Biomedical Research Institute at Virginia Tech Carilion, Roanoke, VA 24016, USA. Email: scottrj@vt.edu Phone: (+44) 540-526-2296

Conflict-of-Interest Statement:

The authors have declared no conflict of interest exists. Peptides generated and used in this manuscript are covered by patent #WO2021021716 (SRJ, BEI).

Abstract:

The gap junction protein connexin 43 (Cx43) is associated with human pathological vascular smooth muscle cell (SMC) proliferation and neointima formation. We previously identified mitogen-activated protein kinase (MAPK) phosphorylation of Cx43 results in binding with the cell cycle protein cyclin E, facilitating neointima formation in mice. However, the specific nature of these interactions and their relevance to human disease have not been elucidated. Using an *ex vivo* human saphenous vein model of neointima formation, we identified increased MAPK-phosphorylated Cx43 and cyclin E in explant tissues. We used peptide arrays to define a cyclin E-Cx43 binding region and generated 'CycliCx', a stearate-linked Cx43 phospho-mimetic peptide. In human coronary artery SMC, CycliCx inhibits platelet-derived growth factor-BB (PDGF-β)-induced changes in Cx43 trafficking and interactions with cyclin E, and stimulation of proliferation. RNAseq analysis identified CycliCx significantly inhibits PDGF-β-induced proliferative pathways in SMC by limiting PDGF-induced early G1/S phase cell cycle progression transcripts. Finally, we show CycliCx limits neointima formation in mice *in vivo* and in *ex vivo* human saphenous vein explants. Our data provide strong evidence for selective targeting Cx43 as a viable therapeutic strategy for preventing neointimal formation in humans.

48 **Introduction:**

49 Atherosclerosis in the coronary artery narrows the vessel lumen, restricts arterial blood flow,
50 affecting more than 20.5 million Americans, making it the primary underlying cause of
51 cardiovascular disease[1]. Surgical interventions, such as coronary artery bypass and
52 percutaneous coronary interventions (angioplasty/stent placement) can be employed to
53 revascularize and alleviate symptoms and risks of coronary artery disease. Of those who undergo
54 surgical revascularization, 16.4% will experience a serious adverse event, including a heart attack
55 or death[2]. This highlights a need for novel therapeutics that can enhance vessel patency following
56 revascularization surgeries.

57 The leading cause of long-term patency issues after coronary artery bypass grafting (CABG) or
58 percutaneous coronary intervention is neointimal hyperplasia[3], which occurs when vascular
59 smooth muscle cells (SMC) in the medial layer of arteries/ vascular conduits dedifferentiate, take
60 on a proliferative and migratory phenotype, and block the vessel intima[3]. Drug-eluting stents are
61 often used to limit neointimal growth, yet these stents use broad antiproliferative agents, which
62 delay vessel healing and necessitate the prolonged use of dual antiplatelet therapy, increasing
63 the risk for clinically significant bleeding[3-5]. As such, identifying mechanisms of neointima
64 development specific to SMC proliferation is essential in developing novel therapeutics.

65 Connexins form hexamers on the plasma membrane, which dock with connexin hexamers on
66 adjacent cells, forming gap junctions, facilitating cell-cell communication[6]. Increasing evidence
67 suggests connexins also regulate cell function in a gap junction-independent manner through
68 protein-protein interactions[7-14]. In SMC, altered Cx43 expression has been associated with
69 neointimal hyperplasia, but the specific role Cx43 plays is currently unresolved, with conflicting
70 studies showing both increased and decreased proliferative states in response to altered Cx43
71 expression[15-19]. Additionally, decreased expression and gap junction signaling are associated with
72 both enhanced and delayed vascular disease progression[15,16,20-22].

73 Nuclear magnetic resonance analysis of the cytoplasmic Cx43 C-terminus reveals two α-helical
74 regions with a randomly coiled structure for the remaining length, forming a flexible protein primed
75 for phosphorylation and protein-protein interactions[23]. In addition, Cx43 contains a long
76 intracellular C-terminus with a high percentage of amino acids (a.a.) that can be post-
77 translationally modified[10,24,25]. The phosphorylation states influence the conformation of the Cx43
78 C-terminus, altering the accessibility of other Cx43 phosphorylation sites and regulating the Cx43
79 protein-protein binding affinity[26]. Our previous study showed in response to platelet-derived
80 growth factor-BB (PDGF-β), Cx43 is phosphorylated by mitogen-activated protein kinases

81 (MAPK) at four of its C-terminal serines[24]. Phosphorylation by MAPK promotes Cx43 binding to
82 the cyclin E protein, which binds with CDK2 to promote G1/S phase cell cycle transition[24,27], and
83 results in SMC proliferation in mice[24]. Our previous data suggested disrupting Cx43-MAPK
84 activation does not compromise the viability of healthy SMC *in vivo,* making it a suitable target for
85 therapeutic intervention[24]. In transgenic Cx43-MAPK phosphorylation-null mice, Cyclin E-Cx43
86 interactions were inhibited, and ligation-induced carotid artery neointima was reduced[24]. Despite
87 this, the binding sites for Cx43 and cyclin E have not been elucidated yet.

88 In the present study, we aimed to define the importance of cyclin E-Cx43 interactions in human
89 vascular tissues during neointima formation, and hypothesized disrupting cyclin E-Cx43 protein-
90 protein interactions could prevent neointima formation. We developed models of *ex vivo* human
91 neointima formation using excess human saphenous veins intended for coronary artery bypass
92 grafts and show cyclin E-Cx43 interactions form during PDGF-β-induced SMC proliferation. We
93 used peptide array techniques to define a 14 a.a., phospho-dependent cyclin E binding site on
94 Cx43 and developed a stearate-linked linear peptide ('CycliCx') to disrupt cyclin E-Cx43
95 interactions. *In vitro* testing demonstrated CycliCx inhibits PDGF-β-induced changes in Cx43
96 localization and phosphorylation state, limits cyclin E-Cx43 interactions, and reduces human SMC
97 proliferation. Transcriptomics data highlighted the CycliCx peptide disrupts PDGF-β-induced gene
98 pathways regulating G1/S phase cell cycle progression in cultured human SMC. Importantly, our
99 data show CycliCx is a potent inhibitor of neointima in mouse and human models. This study is
100 the first to demonstrate specific binding domains for cyclin E-Cx43, show relevance in human
101 disease, and identify a specific molecule targeted to SMC that limits neointima formation.

Results

A human saphenous vein model of neointima formation shows Cx43 MAPK-phosphorylation in new neointima cells. Previous *ex vivo* models of human saphenous vein neointima developed by George et al.[28,29] demonstrated high serum levels promote SMC proliferation and migration to the intimal surface of tissue explants, forming a "new intima" on the surface of the explants. We aimed to adapt this model to examine the effects of PDGF-β-induced proliferation using low serum media (**Figure 1A**). Human saphenous vein tissue explants had no treatment (NT; no PDGF-β) or 14 day treatment (PDGF-β, 50 ng/mL). Histological staining demonstrated an increase in cell layers at the surface of the explants in PDGF-β-treated tissue (**Figure 1B, Supplemental Figure 1**). The appearance of the cells is consistent with the new intima in previously published models for *ex vivo* HSV intimal growth[28,29]. Immunofluorescent staining demonstrated cells in the upper layers of the tissue are transgelin (TGLN) positive SMC, with significant increases in PDGF-β-treated tissues (**Figure 1B, Supplemental Figure 2**). Staining also identified high levels of expression for total Cx43 and cyclin E within these cells, and antibodies specific to MAPK-phosphorylated sites on Cx43[24] highlight PDGF-β promotes Cx43-MAPK phosphorylation (**Figure 1B, Supplemental Figures 3-5)**.

Identification of a binding region between Cx43 and cyclin E and development of the CycliCx peptide. Our previously published data suggest phosphorylation at Cx43-MAPK C-terminal serines (S) regulates protein interactions between cyclin E and the Cx43 C-terminus[24]. However, specific sites of interaction are unknown, and structural modeling of Cx43 is limited. Therefore, we used a peptide array to define the critical binding sites of the Cx43 C-terminus required for binding with cyclin E. Peptide arrays of the full Cx43 C-terminus (a.a. 236-382) were designed with 25 a.a. peptide sequences arranged sequentially, with a five a.a. overlap between each sequence (**Figure 2A**). Arrays were arranged to test a requirement of the Cx43-MAPK serines located at S255/S262/S279/S282 (MK4) on Cx43, using either: non-mutated serines ($Cx43^{wt}$, non-phosphorylated state), mutated alanine ($Cx43^{MK4A}$, non-phosphorylatable state), mutated aspartate ($Cx43^{MK4D}$, phosphorylated state mimic), or native phosphoserine ($Cx43^{MK4pS}$, phosphorylated state). The full-length cyclin E protein was synthesized, as we previously described[24] (**Figure 2B**). Isolated cyclin E proteins were incubated with Cx43 peptide arrays, and binding was detected using antibodies targeting cyclin E (**Figure 2C-D**). Initial peptide arrays identified three potential binding regions in each of the $Cx43^{MK4D}$ and $Cx43^{MK4pS}$ sequences (**Figure 2C-D**). Given consensus between D/pS binding regions, we focused on a.a. 236-301, which were divided into three separate, but overlapping, 25 a.a. peptide sequences: Seq1 a.a.

235-260 (gray), Seq 2 a.a. 254-279 (green), Seq 3 a.a. 276-301 (black) (**Figure 2 E-F**). To test the requirement of single a.a., we prepared arrays using alanine substitutions along the length of each sequence, incorporating phosphorylation of Cx43-MAPK serines where they occurred. These data indicated there was consistent binding when phosphorylation was present in Seq 1 and Seq 2, but no evidence of binding in Seq 3 (**Figure 2G**). Further, single a.a. substitutions did not significantly impact overall binding in Seq 1-2 (**Supplemental Figure 6A**).

Using a truncation mutation peptide array approach, which reduces the sequence length by a single a.a. at a time, we tested variants within the identified short region GVKDRVKGRSD (Peptide-1, 11 a.a.) and longer region LDPSKDCGDPKYAYFNGCSSPT (Peptide-2, 22 a.a.) that showed cyclin E binding (**Supplemental Figure 6B-C**). We synthesized peptides for these sequences conjugated with an N-terminal stearyl group to aid in peptide cellular internalization. Peptides (30 μM) were incubated with cell cycle-stalled primary human coronary artery smooth muscle cells (CASMC) treated with PDGF-β (50 ng/mL) to promote proliferation. We used 5-ethynyl 2´-deoxyuridine (EDU) to label newly synthesized DNA and measured proliferation by flow cytometry. At 48 hours, PDGF-β increased proliferation in CASMC, which was reduced by Peptide 2 without notable cell loss (**Supplemental Figure 6D**). However, Peptide 1 treatment resulted in significant cell loss and was not tested further (**Supplemental Figure 6D**).

Peptide arrays indicated a minimum binding sequence within Peptide 2, between a.a. 254-268, but a loss of signal after removal of Tyrosine 267 (**Figure 2H, Supplemental Figure 6C).** Because of this, we created two peptides. The first peptide, named 'CycliCx', is a 14 a.a. sequence, LDPSKDCGDPKYAY, which showed cyclin E-Cx43 binding. The second control off-target peptide (OT-peptide) is a 15 a.a. peptide, AYFNGCSSPTAPLDP, which represents the immediately adjacent a.a. sequence unable to bind cyclin E. Both peptides were synthesized with an N-terminal stearate to promote cell entry, giving a final design of stearate-LDPSKDCGDPKYAY (CycliCx), and stearate-AYFNGCSSPTAPLDP (OT peptide), which was used as a control treatment throughout this study (**Fig 2H-I**). Because the CycliCx sequence was initially based on the mouse Cx43 sequence, we created a humanized CycliCx peptide, stearate-LDPAKDCGDQKYAY, for testing (**Fig 2I**). We saw no differences between mouse and human CycliCx peptides in effect in cells (not shown). The human CycliCx peptide was used for all future experiments. The two peptides have approximately the same molecular weight and charge. The CycliCx peptide has a sequence predicted MW of 1571 kDa, (1853.22 kDa with stearate group) and a charge of -1, and the OT peptide has a predicted MW of 1586 kDa (1806.01 kDa with stearate group) and a charge of -1 (**Supplemental Figure 6E**).

168 **CycliCx peptide alters Cx43 cellular functions in human CASMC.** Our previous data showed
169 PDGF-β-induced ERK phosphorylation is a key factor in regulating cyclin E-Cx43 protein
170 interactions in mouse primary SMC[24]. To assess ERK activation, human CASMC were treated
171 with PDGF-β (50 ng/mL) to induce proliferation. Treatment with PDGF-β significantly upregulated
172 ERK phosphorylation (pERK) in CASMC (**Figure 3A, Supplemental Figure 7**). Treatment of
173 CASMC with either CycliCx or OT-peptide (30 μM each) did not significantly alter levels of PDGF-
174 β-induced pERK in CASMC (**Figure 3A, Supplemental Figure 7**). In addition, total Cx43
175 expression was not affected by PDGF-β in CASMC; however, CycliCx altered Cx43 western blot
176 protein banding, while OT-peptide had no effect (**Figure 3B, Supplemental Figure 8**). Based on
177 previous reports of phosphorylation states present in each migrating band, we assessed Cx43
178 protein kinase-C (PKC) phosphorylation at Cx43-S368 (Cx43-pS368). These data highlight
179 CycliCx significantly increases the phosphorylation at Cx43-S368 in CASMC (**Figure 3B,**
180 **Supplemental Figure 8**). While most experiments in cells were performed at 16 hours, we found
181 CycliCx produced alterations in Cx43 as early as 3 hours (**Supplemental Figure 9**).

182 To assess Cx43 expression and localization, we performed immunofluorescence of cultured
183 CASMC and identified punctate staining characteristic of Cx43 which was not significantly altered
184 by treatment with PDGF-β or PDGF-β+OT peptide (**Figure 3C, Supplemental Figure 10**). In
185 PDGF-β + CycliCx-treated cells, Cx43 staining punctates were significantly reduced and staining
186 appeared more diffuse (**Figure 3C, Supplemental Figure 10**). Membrane biotinylation
187 experiments demonstrated PDGF-β and PDGF-β +OT peptide treatments reduced Cx43
188 expression at the plasma membrane. CycliCx inhibited the PDGF-B-induced removal of Cx43
189 from the plasma membrane (**Figure 3D, Supplemental Figure 11**). To test if CycliCx altered gap
190 junction signaling, we performed lucifer yellow scrape load dye transfer assays. We found CycliCx
191 inhibited Cx43 gap junction communication compared to controls (**Figure 3E, Supplemental**
192 **Figure 12**). Finally, we tested if CycliCx could inhibit interactions between Cx43 and cyclin E. Co-
193 immunoprecipitation assays demonstrate PDGF-β treatments increased cyclin E-Cx43 complex
194 formation in human CASMC ([24]), but were significantly reduced by treatment with CycliCx (**Figure**
195 **3F, Supplemental Figure 13**).

196 **CycliCx peptide inhibits PDGF-β-induced proliferation by blocking G1/S phase cell cycle**
197 **transition.** To test if the peptide alters the proliferation of SMC in a human model, we assessed
198 PDGF-β-induced proliferation in human CASMC by EDU flow cytometry. We found PDGF-β
199 significantly upregulated CASMC proliferation, which was inhibited by treatment with CycliCx but
200 not OT-peptide. (**Figure 4A**, **Supplemental Figure 14**). Bulk RNA sequencing of CASMC treated

201 revealed PDGF-β+CycliCx altered the transcript expression of more genes than PDGF-β+OT
202 peptide when compared with PDGF-β alone (**Figures 4D-E**). Pathway enrichment analysis using
203 the Gene Ontology (GO) database demonstrated a significant upregulation of pathways involved
204 in cell cycle progression and mitotic nuclear division in PDGF-β-treated compared to control
205 CASMC, indicating CASMC differentiation into a pro-proliferative phenotype (**Figure 4F**). The
206 addition of the CycliCx peptide resulted in significantly decreased enrichment of these same
207 proliferative pathways when compared to PDGF-β treatment alone and to PDGF-β+OT peptide-
208 treated CASMC (**Figure 4F, Supplemental Figure 16**).

209 Furthermore, CycliCx treatment significantly blunted the PDGF-β-induced transcript expression
210 of large arrays of genes involved in 'cell cycle G1/S phase transition' (GO:0000082; **Figure 4G**),
211 'cell cycle G2/M phase transition' (GO:0044839), and 'mitotic nuclear division' (GO:0140014;
212 **Supplemental Figure 16**). Importantly, PDGF-β+OT peptide treatment did not significantly blunt
213 the PDGF-β-induced expression of these genes. We next interrogated the expression of key
214 regulatory genes at each phase of the cell cycle (**Figure 4G**; **Supplemental Figure 17**) and found
215 CycliCx treatment had no effect on the PDGF-β-induced expression of Ccnd1 (Cyclin D1) and
216 CDK4, which regulate early G1 progression, but partially blunted CDK6 and Cdkn2c (p18)
217 expression (**Supplemental Figure 17**). Although CycliCx impairs binding of Cyclin E, it had no
218 effect on Ccne1 (cyclin E1) gene expression (**Figure 4H)**. However, CycliCx significantly blunted
219 the PDGF-β-induced increase in the expression of G1/S phase transition promoters CDK2 and
220 E2f1 and partially reversed the PDGF-β-induced decrease in expression of G1/S phase transition
221 inhibitors Tp53 (p53) and Cdkn1a (p21) (**Figure 4H**; **Supplemental Figure 17**). Finally, we
222 assessed late G2/M phase regulatory genes and found CycliCx inhibited the PDGF-β-induced
223 increase in Ccna2 (Cyclin A2) and Cdk1, while OT peptide treatment had no effect (**Figure 4H**;
224 **Supplemental Figure 17**). Last, CycliCx did not alter the expression of Cx43, Timp1 (**Figure 4H**),
225 Timp3, and Il1b, or the downstream effector kinases Mapk3 (Erk1) and Mapk1 (Erk2;
226 **Supplemental Figure 18**). Smooth muscle contractile markers were decreased by treatment with
227 PDGF-β, but these do not appear to be directly altered by treatments with CycliCx or OT peptide
228 (**Supplemental Figure 19**).

229 **CycliCx peptide disrupts neointima formation in mice and human blood vessels.** To test
230 CycliCx *in vivo*, we combined carotid ligation surgeries in mice with the application of peptides
231 mixed in pluronic gel to the outside of carotids (**Figure 6A**). We found significant neointima
232 formation in pluronic controls and OT peptide-treated mice compared with sham ligation mice
233 (**Figure 6A**). Treatment with CycliCx peptide significantly inhibited ligation-induced neointima in

234 mice and was not significantly different from sham control mice (**Figure 6A, Supplemental**
235 **Figure 20)**. We found no sex differences in mice in terms of neointima formation or the effect of
236 the peptide, and data shown represent both male and female mice (**Supplemental Figure 20**).
237 We then tested the effect of CycliCx in PDGF-β-induced neointima formation in ex vivo human
238 saphenous veins. As shown in **Figure 1B and Supplemental Figures 1-5**, PDGF-β promotes
239 the formation of SMC-derived new intima regions at the surface of tissue explants. This is
240 significantly increased when compared with no treatment at 14 days and is unaffected by OT-
241 peptide treatments (**Figure 6B, Supplemental Figures 1-5)**. In *ex vivo* human saphenous veins,
242 CycliCx significantly reduces the presence of SMC in the intimal region of explants, suggesting
243 inhibition of neointima formation (**Figure 6B, Supplemental Figures 1-5)**.

244 **Discussion**

245 Targeted therapies to address the mechanisms of neointima formation are needed to reduce the
246 risk of stent/bypass failure. Our previously published data identified phosphorylation of Cx43 at
247 its C-terminus MAPK residues regulates SMC proliferation and neointima formation in mouse
248 models[24]. This control of SMC proliferation is dependent on interactions between the Cx43 C-
249 terminus and cell cycle-regulating protein cyclin E[24]. In the present study, we defined for the first
250 time the binding region of cyclin E on Cx43 and demonstrated MAPK phosphorylation sites within
251 this binding region are required for direct cyclin E-Cx43 interactions. We developed the CycliCx
252 peptide, which mimics a short 14 a.a phosphorylated region of the Cx43 C-terminus within the
253 MAPK region, and was designed to inhibit cyclin E-Cx43 binding. Our data highlight CycliCx alters
254 Cx43 localization, signaling, and trafficking while limiting cyclin E binding with Cx43. Using a
255 transcriptomic approach, we found CycliCx significantly blunts PDGF-β-induced cell cycle
256 progression, leading to reduced proliferation in cultured human CASMC. Finally, we showed
257 CycliCx significantly alters neointima formation in models of disease in mouse and human tissues.
258 This work establishes critical binding sites on Cx43 required for SMC proliferation and identifies
259 Cx43 as a viable therapeutic target for the prevention of human neointima formation.

260 Current strategies for mitigating neointima formation after stenting procedures primarily include
261 the use of non-cell-specific drugs such as the Rapamycin analogs, Everolimus and Zotarolimus.
262 These drugs work by targeting mTOR signaling, a pathway essential for protein, nucleotide, and
263 lipid synthesis, ultimately regulating cell growth and division[30]. Although mTOR inhibitors can stop
264 the pathological proliferation and migration of SMC, which form neointima, they present a risk to
265 other cell types in the vasculature, particularly endothelial cells that protect the vessel from platelet
266 aggregation and ultimately thrombus formation[4]. Our recent investigation revealed significant
267 endothelial damage caused by standard preservation techniques during coronary bypass surgery,
268 and highlighted the need for endothelial healing[31]. Targeting cyclin E-Cx43 interactions disrupts
269 a key signal required for pathological SMC growth without impacting cell viability or global mTOR
270 signaling. As such, this is a promising strategy for targeting neointima formation/restenosis
271 without impacting healthy cellular healing functions and adversely impacting patient health.

272 Emerging research reveals Cx43 proteins can act independent of forming cell-cell gap junction
273 channels to control cellular functions[7-13]. We previously found Cx43 interacts with the cell cycle
274 control protein cyclin E in mouse SMC *in vitro* and *in vivo*. Cyclin E tightly controls G1/S phase
275 cell cycle transition, which is critical for pathological SMC proliferation[27,32]. Our data in human
276 saphenous vein explants showed both Cx43 and cyclin E are expressed in the new intima layers

277 after PDGF-β stimulation, suggesting a role for Cx43 in the SMC proliferation in these tissues.
278 Given our previous evidence that blocking these interactions is important in mouse neointima
279 formation, we set out to define the role of cyclinE-Cx43 interactions in human neointima and SMC
280 proliferation.

281 This is the first study to comprehensively define the location of cyclin E-Cx43 binding. We
282 identified two regions on the Cx43 C-terminus with consistent cyclin E binding activity and used
283 these to generate Cx43 mimetic peptides. The first region, used to generate peptide-1, spans
284 Cx43 a.a. 235-245, which does not encompass any reported Cx43-MAPK phosphorylation sites.
285 This peptide is highly similar to the Cx43 mimetic peptide juxtamembrane 2 (JM2)[33]. The JM2
286 peptide sequence is designed to cover the binding region between Cx43 and microtubule subunit
287 β-tubulin[33]. JM2 enhances the Cx43 β-tubulin interactions, reduces Cx43 trafficking to the plasma
288 membrane, and reduces Cx43 hemichannel ATP release[33,34]. In our *in vitro* model of PDGF-β-
289 induced CASMC proliferation, the overlapping peptide 1 resulted in cell death, and further testing
290 of this peptide was not performed, as our goal is to limit CASMC from entering a proliferative
291 phenotype while maintaining vessel health. This is in line with previous work in 4T1 tumor cells,
292 in which JM2 was found to induce ROS-mediated apoptosis by disrupting mitochondrial
293 trafficking[35]. However, no JM2 cytotoxicity was reported in healthy cultured human microvascular
294 endothelial cells[33]. Conflicting cellular responses to the JM2/peptide 1 sequences could arise from
295 differences in cell types, with CASMC more susceptible than the endothelium. Duration of
296 treatment and dose may also be responsible for the differential effects reported.

297 The second cyclin E-Cx43 binding region, used to generate peptide 2 and the final CycliCx
298 peptide, spans Cx43 a.a. 254-275, with phosphomimetic aspartate mutations at the known Cx43-
299 MAPK phosphorylation sites, S255 and S262. Cyclin-dependent kinase 1 (CDK1) and ERK5 are
300 implicated in the phosphorylation of Cx43 at one or both of the S255 and S262 sites[36-38], which
301 correlate with gap junction internalization and cell division[24,36-39]. To include an appropriate control
302 condition when testing the CycliCx peptide, we developed the OT peptide based on the sequence
303 immediately adjacent to CycliCx (Cx43 a.a. 266-280). The OT peptide contains the known Cx43-
304 MAPK phosphorylation site Cx43 S279 (but not the S282 site), and in line with the CycliCx
305 peptide, the OT peptide contains a phosphomimetic aspartate at its corresponding residue and
306 an identical N-terminal stearate group. The OT peptide sequence was selected as a control due
307 to its proximity to CycliCx and lack of cyclin E binding activity. The OT peptide is similar to the first
308 15 a.a. of the 18 a.a. TAT-Cx43266-283 peptide published by Gangoso et al., with the exception
309 of the a.a. 279 serine to aspartate mutation[7,40]. TAT-Cx43266-283 is a Cx43 mimetic based on

310 the cSRC binding domain. cSRC perpetuates cell proliferation in some cancers, and evidence
311 suggests binding with Cx43 inactivates cSRC and limits cancer growth. It is thought TAT-
312 Cx43266-283 binds cSRC directly, mimicking the effect of full-length Cx43 and limiting
313 glioblastoma growth in culture and *in vivo*[7,40]. In the present study, the OT peptide did not inhibit
314 SMC proliferation or neointima formation. Due to the similarity between TAT-Cx43266-283 and
315 our OT peptide, it is possible our OT peptide is lacking critical a.a. for cSRC binding, the aspartate
316 mutation within the OT peptide prevents cSRC binding, or cSRC does not play a significant role
317 in injury-induced proliferation in SMC.

318 Proposed mechanisms of action for previously published Cx43 mimetic peptides include binding
319 between the Cx43 mimetic and a physically interacting protein, or direct binding between the Cx43
320 mimetic and Cx43 itself[7,40,41]. Our peptide array data demonstrate sequences for CycliCx and the
321 cyclin E protein can bind directly. Although we do not present direct evidence of CycliCx-Cx43
322 interactions, CycliCx induced a shift in Cx43 molecular weight attributable to an increase in Cx43-
323 pS368, a known PKC phosphorylation site. Cx43-pS368 phosphorylation is associated with
324 control over gap junction open/closed states and has been observed with other Cx43 mimetic
325 peptides, a phenomenon we summarized in our previously published review[42]. For example, the
326 Cx43 mimetic peptide αCT1, developed by the Gourdie lab to disrupt Cx43/ZO-1 interactions,
327 binds directly to the Cx43 C-terminus, causing an increase in Cx43-PKC phosphorylation[41].
328 Mutating αCT1 to interact only with ZO-1 and not directly with Cx43 did not produce increases in
329 Cx43-pS368, indicating direct Cx43 binding is required for αCT1-induced Cx43-pS368 [41]. As
330 CycliCx induces a similar phosphorylation shift, it is possible CycliCx is also capable of directly
331 binding the Cx43 protein.

332 Cyclin E exerts control over the cell cycle via binding with its kinase CDK2. Although the complete
333 mechanism of action of cyclin E-CDK2 is uncertain, it is known this complex translocates from the
334 cytoplasm to the cell nucleus to phosphorylate the retinoblastoma protein and exert its effect on
335 cell division[43-46]. In our previous studies, cyclin E-Cx43 complexes are initially present in the cell
336 membrane but bind Cx43 and are removed after prolonged PDGF-β treatment, demonstrating
337 Cx43 can accompany cyclin E-CDK2 during translocation[24]. In the present study, CycliCx
338 treatment retained Cx43 at the cell membrane after PDGF-β treatment, likely attributable to the
339 shift toward Cx43-pS368 phosphorylation, which is associated with stabilizing Cx43 at the
340 membrane[47,48]. Therefore, it is possible Cx43 is required to chaperone cyclin E to the cell nucleus
341 to progress the cell cycle and induce proliferation, and disrupting the cyclin E-Cx43 complex
342 interaction and trafficking prevents this.

343 In line with this, our transcriptomic data suggest CycliCx treatment blunts the PDGF-β-induced
344 increase in transcript expression of critical cell cycle promoter genes downstream of the cyclin E-
345 CDK2 complex. Cyclin E-CDK2 primarily regulates the G1/S phase transition of the cell cycle[27].
346 Indeed, there was little change in the expression of genes involved in the regulation of the early
347 G1 phase of cell cycle progression with CycliCx treatment, while CycliCx significantly blunted the
348 PDGF-β-induced regulation of G1/S phase transition and subsequent G2/M phase transition and
349 M phase genes. This suggests CycliCx targets cyclin E to arrest the cell cycle during the G1/S
350 phase transition.

351 In addition to halting pathological SMC proliferation and neointima formation, it is important to
352 examine potential off-target effects of the CycliCx peptide. We found many PDGF-β downstream
353 transcription targets unrelated to cell cycle, such as tissue inhibitors of metalloproteases (TIMPs)
354 and interleukins, were not affected by the CycliCx peptide. Our investigation also revealed a
355 reduction in gap junction communication following CycliCx treatment. This may be attributable to
356 the observed increase in Cx43-pS368, which is associated with gap junction closure[49,50].
357 Interestingly, PDGF-β also induced gene expression of Cx40, but this increase in expression was
358 reduced after treatment with CycliCx. Together, these data demonstrate CycliCx treatment
359 specifically inhibits PDGF-β-induced pathological SMC cell cycle progression without significant
360 disruption to other cell signaling pathways.

361 A caveat to this study is the use of veins over arteries in testing CycliCx treatment in human
362 tissues. In modern clinical practice, the internal mammary or radial arteries are preferred for
363 coronary bypass surgeries over the saphenous vein due to lower levels of neointima formation[51-
364 53]. Even so, the saphenous vein is still used more often than any other vessel for coronary bypass
365 when additional bypass conduits are required[54]. As such, testing CycliCx in venous tissue is highly
366 relevant to surgical practice. Currently, we are unable to trace the half-life of the CycliCx peptide
367 due to a lack of available antibodies to CycliCx and the mechanism of synthesizing the peptide.
368 The CycliCx peptide is synthesized with an N-terminal stearate group, limiting our ability to add a
369 reporter such as GFP to the C-terminus. Attempts to add 6xHis tags to the peptide resulted in
370 insoluble peptides and were not viable for testing. However, our data show clear effects in vivo in
371 mice at 14 days, and our in vitro studies show CycliCx effects appear around 3 hours and remain
372 at >16 hours, suggesting a peptide with good stability, although this remains to be fully elucidated.
373 Our data also shows CycliCx limits gap junction signaling; thus, we are unable to distinguish gap
374 junction and connexin-mediated effects directly in this study. However, our previous study found
375 that Cx43-gap junction signaling did not play a significant role in PDGF-β-induced SMC

376 proliferation in mice[24]. The CycliCx peptide may therefore also act as a promising tool for the
377 specific regulation of gap junction signaling, which is not currently available.

378 In conclusion, we show targeting Cx43 and cyclin E interactions with the novel Cx43 mimetic
379 peptide CycliCx limits SMC proliferation and neointima formation. The findings from this study
380 highlight new pathways important in neointima formation, which could be targeted to improve
381 patency in human revascularization strategies. While our study focuses on pathological
382 proliferation in SMC in blood vessels, Cx43 has been implicated in the progression of various
383 proliferative diseases[55]. As our data suggests, CycliCx targets a Cx43-dependent pathological
384 proliferative mechanism. Future research will also focus on exploring the potential of CycliCx
385 treatment in other proliferative diseases.

386 **Methods**

387 **Sex as a biological variable**

388 Male and female mice were used to assess sex as a biological variable in animal studies. Our
389 data do not show differences in cell pathology or neointima formation in male vs female mice, and
390 the results report combined data for both male and female mice. The sex of the individual mice is
391 indicated in **Supplemental Figure 20**.

392 **Key Resources:** Reagents, materials, and antibodies are all listed in **Supplemental Table 1**

393 ***Ex vivo* human saphenous vein model of neointima formation:** We adapted a previously
394 described *ex vivo* model of human saphenous vein neointima formation developed by George et
395 al.[28,29]. At the end of surgical procedures for coronary artery bypass graft, excess, normally
396 discarded saphenous vein tissue was collected. De-identified specimens from Carilion Clinic
397 cardiovascular patients were processed within 1 hr of the end of surgery. Tissues greater than 2
398 inches in length, free from visible valves and branch regions, were used in the study. Tissues
399 were placed into a container of harvest media (20 mM HEPES-buffered RPMI-1640, 0.225 mg/mL
400 papaverine hydrochloride, 5 µg/ml amphotericin B, 20 IU/mL sodium heparin). Samples were
401 transferred to a wash media (20 mM HEPES Buffered RPMI-1640 with 2 mM L-Glut, 8 µg/mL
402 gentamicin, 1 IU/mL penicillin, and 1 µg/mL streptomycin). Tissues were cut into four consecutive
403 explant sections (corresponding to treatments) and pinned on 6-well plates containing Sylgard
404 184 elastomer (**Figure 1**). Explants were maintained in a low-serum media (bicarbonate buffered
405 RPMI-1640, 2 mM L-Glut, 8 ug/mL gentamicin, 1 IU/mL penicillin, 1 µg/mL streptomycin, and 2%
406 FBS). The four treatment groups corresponding to four sections were: 1) no treatment; 2) PDGF-
407 β (50 ng/mL, Millipore #01-305); 3) PDGF-β (50 ng/mL) plus OT peptide (30 µM); and 4) PDGF-
408 β (50 ng/mL) plus CycliCx peptide (30 µM). Media were changed each day for 14 days. At the
409 end of the experiments, tissue explants were fixed *in situ* in 4% PFA at 4°C overnight. To preserve
410 integrity, tissues were encapsulated in 3% agarose before tissue processing and paraffin
411 embedding by the FBRI Histology Core. Comparisons were made to PDGF-β treatment or to
412 PDGF-β+OT peptide and PDGF-β+CycliCx treatments for changes in new intima formation.

413 **Cx43 peptide arrays for cyclin E binding:** SPOT synthesis of peptides and overlay experiments
414 were carried out as described[56]. Full-length cyclin E-GST protein was synthesized as previously
415 described by us[24]. Cyclin E-GST proteins for arrays were isolated using anti-GST beads, spin
416 concentrated (Amicon, 10K MWCO, Millipore #UFC901008), and buffer exchanged to PBS 125
417 mM NaCl, pH 6.5 on PD10 columns (Millipore #GE17-0851-01). Peptide arrays were initially
418 bathed in 100% ethanol, equilibrated in PBS-Tween (PBST, 125 mM NaCl, 0.1% tween, pH 6.5)

419 for 10 min, then blocked in PBST-5% block (PBST with 5% milk) at room temperature for 2 hr.
420 Arrays were washed in PBST, then incubated with cyclin E proteins (2.86 mg/mL) in PBST-1%
421 block (1% Milk). Binding on arrays was detected using (cyclin E primary antibodies) in PBST-1%
422 block, followed by secondary detection using rabbit HRP (Thermo Fisher #31458) in PBS-T-1%
423 block for 1 hr at room temp, then developed by chemiluminescent substrate (SuperSignal, Thermo
424 Fisher # 34579) on x-ray film in a dark room. Developed films were scanned for image analysis
425 (cyclin E, Odyssey, LiCor). Arrays were imaged using UV to provide imaging of total peptides
426 (Odyssey, LiCor). Sequences for the truncation mutation array can be found in **Supplemental**
427 **List 1.**
428 **Peptides:** Peptides used in the studies were designed based on the peptide array minimal binding
429 sequences shown in **Figure 2**. Peptides were synthesized with an N-terminal stearate group to
430 improve cellular uptake[57]. Peptide final sequences used in the study are CycliCx: stearate-
431 LDPSKDCGDPKYAY and Off-Target (OT) peptide: stearate-AYFNGCSSPTAPLDP. Peptide
432 properties are described in **Supplemental Figure 6**. Patent #WO2021021716: "Compositions
433 and methods for inhibiting neointimal formation" covers the discovery and use of peptide (CycliCx)
434 and control peptides. Peptides were commercially synthesized (ThermoFisher custom peptide
435 synthesis services) to >80% purity. Peptides were reconstituted at room temperature in sterile
436 PBS (for cell culture) or saline (for *in vivo*) to a concentration of 2 mM and stored at -80°C for use.
437 Peptides used in cell culture and explant culture experiments were prepared to a final
438 concentration of 30 μM in media. Peptides for *in vivo* applications in mice were prepared to a
439 concentration of 200 μM in a pluronic gel (35% final concentration), with 50 μL of the pluronic gel
440 applied around the ligated carotids.

441 **Animals:** All mice were cared for under the provisions of the Virginia Tech Animal Care and Use
442 Committee and followed the National Institute of Health guidelines for the care and use of
443 laboratory animals. All studies were performed in C57BL6/J mice; strain number #000664,
444 purchased from Jackson Labs. Mice were bred in-house and used between 12-14 weeks of age.

445 **Carotid ligations and carotid Pluronic gel applications in mice:** Permanent 14-day carotid
446 ligations were used to promote neointima in mice, as we previously described[24]. Mice were,
447 anesthetized using isoflurane, placed on a surgically sterile heating pad with isoflurane, and the
448 neck area cleared of hair and sterilized. Mice received analgesic (Ethiqa 0.5 mL) proximal to the
449 surgical site. An incision was made in the neckline of the mice, carotid exposed, and a 6/0 suture
450 was secured to the carotid immediately before the bifurcation. In sham control mice, a 6/0 suture
451 was passed under the exposed carotid and then removed. In ligated and sham mice, carotids

452 were elevated, and cold Pluronic gel (50 μL) was applied evenly around the carotid. Carotids were
453 held in place for around 10 seconds until the Pluronic gel solidified (as we previously described)[58].
454 The surgical site was then closed, and the skin sutured, followed by post-operative recovery.
455 Comparisons were made to surgical controls (sham) and OT peptide controls.

456 **Pluronic gel preparation and application in mice.** A 50% Pluronic gel stock was made by
457 adding 3 g of Pluronic powder to 3 mL of ice-cold sterile saline and mixing under cold conditions
458 until dissolved. Pluronic gels were sterilized by autoclaving. For surgeries, Pluronic stocks (50%)
459 were mixed with sterile saline or with peptides in sterile saline to achieve a final concentration of
460 35% Pluronic. Samples were maintained on ice to maintain a liquid form until ligations were placed
461 in the mouse carotid, then 50 μL of Pluronic was applied using a positive displacement pipette to
462 the surgical site. The 35% Pluronic gels solidify around the carotid at body temperature in mice
463 prior to closing the surgical site.

464 **Cell culture.** Primary human CASMC were sourced from American Type Culture Collection
465 (ATCC, #PCS-100-02), ThermoFisher (#C0175C) and Lonza (#CC-2583). Initial stocks of cells
466 were thawed and maintained in vascular smooth muscle cell basal media (ThermoFisher #M231-
467 500) containing smooth muscle growth serum (SMGS, ThermoFisher # S00725). Cells were
468 maintained between 70-90% confluency in culture for up to 16 cell divisions. For experiments,
469 $5x10^4$ CASMC per mL were plated in each well of a six-well plate. CASMC were serum starved
470 to stall cell cycle by washing in PBS and then incubating with vascular smooth muscle cell basal
471 media containing 2% FBS for 72 hr prior to treatments. Media were changed every 48 hours.
472 Stalled CASMC were induced with PDGF-β (50 ng/mL) and harvested at 16 hr for western blot or
473 48 hr for flow cytometry of proliferation. For peptide treatments, cells were treated simultaneously
474 with PDGF-β (50 ng/mL) and peptide (30 μM).

475 **Flow cytometry:** For studies of proliferation, CASMC were treated with 5-ethynyl-2'deoxyuridine
476 (EDU, Thermo Fisher, #C10425) at the same time as PDGF-β and peptide treatments. At the end
477 of experiments, CASMC were trypsinized, centrifuged (700 rpm, 5 min), then resuspended in 0.5
478 mL PBS. Cells were fixed by adding 70% ethanol while vortexing. EDU detection was performed
479 as per the manufacturer's instructions. Flow cytometry data were collected using a BD Accuri C6
480 flow cytometer, and data analyzed using FlowJo software. Proliferation was calculated as a
481 percentage of EDU-positive cells to total cells.

482 **Imaging and analysis:** Histological imaging was completed on a Nikon Ci-L histology microscope
483 using tile scan functions to capture whole tissues. Data for the quantification of neointima was
484 performed by a researcher blinded to sample identification. All immunofluorescent images were

485 captured using Nikon NIE confocal microscope (A1, with resonance scanning). Single images,
486 maximum intensity Z-stack projection, along with tile scanning, was used to visualize samples. All
487 quantitative analysis was performed using NIS Elements Advanced Research software (Nikon).
488 To analyze new intima in TGLN stained tissues, a line (16pt) was drawn at the luminal edge of
489 the tissues using NIE software using the signal intensity tool. Background signal was set for
490 individual images based on tissue autofluorescence, and the area under the curve (AUC) for the
491 TGLN signal was divided by the length of the tissue. 5-6 images were taken across each tissue,
492 and the AUC was averaged for these values. For each HSV experiment, consecutive samples
493 are used, and a fold change to the individual patient NT sample TGLN signal was made to show
494 changes.

495 **Immunofluorescence:** Tissues fixed in 4% PFA were embedded in paraffin and sectioned.
496 Antigen retrieval was performed (Universal R, antigen retrieval solution, Electron Microscopy
497 Solutions) on deparaffined slides containing tissue sections and tissues blocked in a solution of
498 PBS, 0.1% NP-40 substitute, 1% BSA, where the appropriate blocking solution contained anti-
499 goat serum. Primary antibody incubations were performed overnight at 4ºC, samples washed,
500 and secondary antibodies applied.

501 **Scrape load dye transfer (SLDT) assays:** CASMC were grown as described in wound healing.
502 CASMC were treated with PDGF-β and peptides for either 6 hr or 16 hr. Cells were washed in
503 PBS with calcium and magnesium, and scratch wounds were created using a #10 scalpel. Cells
504 were then incubated with the gap junction permeable Lucifer Yellow (457 mw, final concentration
505 0.05%, Thermo #2790937) and gap junction impermeable Rhodamine Dextran 647 (10,000 mw,
506 final concentration 100 µg/mL ThermoFisher #2860812) for 5 min. Cells were then washed in
507 PBS three times, fixed in 4% PFA for 20 min at room temperature, washed in PBS, and imaged
508 for dye transfer (Nikon A1 confocal). Analysis of dye transfer area for each condition was
509 performed using NI Elements Advanced Research (**Supplemental Figure 12**). Normalized data
510 (to length) was presented as Area/Length of dye transfer.

511 **Western blotting and membrane protein biotinylation and coimmunoprecipitation:** Western
512 blotting, cell surface biotinylation, and co-immunoprecipitation studies were performed as we
513 previously described[24,59]. Proteins for western blotting and cell surface protein biotinylation were
514 harvested in PBS lysis buffer containing 5 mM EDTA, 0.5% sodium deoxycholate, 0.5% NP-40
515 substitute, 1 mM sodium orthovanadate, 10 mM sodium fluoride protease inhibitor cocktail (1:100,
516 Millipore #P8340), phosphatase inhibitor cocktail 2 (1:100, Millipore #P5726), phosphatase
517 inhibitor cocktail 3 (1:100, Sigma #P0044). For co-immunoprecipitation, 10 mM n-

518 ethylmethylamine (Millipore, #291145) was added to the lysis buffer. Protein samples were
519 quantified by BCA assay before loading, and equal loading was confirmed using β-tubulin and
520 total protein assay (Total protein stain, LiCor). Membranes were developed using LiCor secondary
521 antibodies, and imaged on a LiCor Odyssey scanner. Expression analysis was performed using
522 Image Studio (LiCor). Values were normalized to total protein stain or β-tubulin, and changes
523 were calculated as a fold change compared to non-treated controls.

524 **Bulk RNA sequencing.** CASMC were plated, stalled for 72 hr and treated with PDGF-β and
525 peptides overnight. Human CASMC were washed 2x in ice-cold PBS and then lysed in 350 µl of
526 RLT lysis buffer. RNA was harvested (RNeasy Micro Kit, Qiagen #74004) according to the
527 manufacturer's instructions, including the optional DNA removal step. Extracted RNA was
528 quantified using a NanoDrop One spectrophotometer (Thermo Fisher, USA). Aliquots of RNA (1.5
529 µg) were then diluted to equal concentrations (75 ng/µl) in RNase-free water.

530 RNA integrity analysis, library preparation, sequencing, raw read count generation, and
531 differential gene expression analysis were performed commercially by Novogene (Sacremento,
532 CA, USA) using their Human mRNA Sequencing pipeline. Full parameters, protocols, and quality
533 control reports are available on request, but are explained briefly below:

534 RNA integrity was assessed using the 5400 Fragment Analyzer System (Agilent Technologies,
535 CA, USA). mRNA library preparation was performed with poly A enrichment and library quality
536 was verified using Qubit assay for quantification, Agilent Bioanalyzer for size distribution, and
537 qPCR for molarity using adaptor-specific primers. Sequencing was performed on the NovaSeq X
538 Plus (Illumina, USA) platform with 150 bp paired end reads and a minimum of 6 G raw data. Raw
539 sequencing data in FASTQ format were cleaned using custom in-house (Novogene) Perl scripts.
540 Reads with adapter contamination, reads containing more than 10% uncertain nucleotides, and
541 reads in which more than 50% of bases had a quality (Q) score below 5 were removed. At this
542 point, an outlying sample in the PDGF-β group was removed from all further analysis due to
543 significant AT/GC content separation (**Supplemental Figure 15).** Reads were then aligned to the
544 human genome using 'HISAT2' (v2.0.05). Raw read counts were generated using 'featureCounts'
545 (v1.5.0-p3). Fragments Per Kilobase of transcript per Million mapped reads (FPKM) was derived
546 from raw data by Novogene and used to calculate Pearson's correlation coefficient to assess intra
547 group and between group variability, and hierarchical clustering. However, for all downstream
548 analysis raw count normalization was performed using 'DESeq2' (v1.44.0) in the R statistical
549 analysis program (v4.4.1). Gene symbols were extracted based on provided Ensembl ID using
550 'clusterProfiler' (v4.12.0) and 'org.Hs.eg.db' (v3.19.1). 'DESeq2' normalized counts were $\log_2$

551 transformed to ensure a normal distribution. Euclidean distances were then calculated and
552 principal component analysis (PCA) was performed using 'dist()' and 'prcomp()', respectively, in
553 base R.

554 Differential gene expression analysis was performed by Novogene for every possible combination
555 of sample groups using 'DESeq2' (v.1.20.0) with Benjamini-Hochberg multiple comparison
556 adjustment. An adjusted p-value (padj) < 0.05 and an $|\log_2(FC)| > 0$ was set as the threshold for
557 differentially expressed genes (DEGs). Volcano plots displaying $-\log_{10}(padj)$ and $\log_2(FC)$ were
558 generated in R.

559 Pathway enrichment analysis was performed on DEGs with a padj < 0.05 with 'clusterProfiler' in
560 R using the Gene Ontology (GO) database. GO terms with a padj < 0.05 following Benjamini-
561 Hochberg multiple comparison adjustment were considered statistically significantly enriched.
562 Separate pathway enrichment analysis was performed for upregulated DEGs ($\log_2(FC) > 0$) and
563 downregulated DEGs ($\log_2(FC) < 0$). Individual pathway heatmaps were generated by extracting
564 'DESeq2' normalized counts for all DEGs (when comparing PDGF-β+CycliCx to PDGF-β+OT
565 peptide) in indicated statistically significantly enriched pathways and calculating a gene
566 expression z-score for each sample. Data were then visualized using 'pheatmap' (v1.0.12).

567 To interrogate changes in expression of single genes, 'DESeq2' normalized counts were
568 extracted, and the mean normalized counts were plotted in GraphPad Prism 10. A 1-way ANOVA
569 followed by Tukey's multiple comparison testing was performed to assess changes in gene
570 expression between groups. Unless otherwise stated, RNA sequencing data were visualized
571 using 'ggplot2' (v3.5.1).

572 **Statistical analysis**

573 Statistical analysis was performed using Prism version 10.4.2. Samples were assessed for normal
574 distribution using a Shapiro-Wilk test, and outliers were identified using the Prism robust
575 regression and outlier removal (ROUT) test (Q =1%). 1-way or 2-way multiple comparison ANOVA
576 followed by Tukey or Dunnett post-test was used for comparisons between >2 groups. The t-test
577 was used for comparisons of 2 treatment groups. Kruskal-Wallis and Mann-Whitney non-
578 parametric tests were used for groups that did not display normal distribution. A minimum of n=3
579 was used for all statistical analyses, and n values for each experiment are stated in the figure
580 legends. P values are shown for all statistical analyses, with a P value of less than 0.05 considered
581 significant. Data represent mean ± SD.

582 **Approval for the use of human excess vascular tissues.** The Institutional Review Board (IRB)
583 at Carilion Roanoke Memorial Hospital reviewed and approved the use of de-identified human
584 saphenous vein tissues normally discarded at the end of coronary artery bypass graft surgeries.
585 The Carilion Clinic IRB determined the research does not meet the definition of human subject
586 research as outlined in 45 CFR 46.102(d). Patient data, health data, and identifiable information
587 were not included with specimens.

588 **Data availability**

589 All data generated and used for analysis and original data sets are freely available for further
590 analysis

591 **Author contributions**

592 MWS, MCR, MJ, GSB, BEI, and SRJ designed research studies; MWS, MCR, XL, FI, MRL, KR,
593 RCJ, AM, CLD, AKB, MJ, GSB, and SRJ conducted experiments and acquired data; MWS, MCR,
594 XL, KR, RJ, AM, CLD, GSB, BEI and SRJ analyzed data; PDL provided reagents; MWS, MCR,
595 BEI and SRJ wrote the manuscript; All authors approved the final version of the manuscript. A
596 coin flip decided the listed order of co-first authors MWS and MCR; both authors contributed
597 equally.

598 **Acknowledgments**

599 We gratefully acknowledge the resources and services provided by Dr. Clare Dennison, at the
600 FBRI Histology Core Facility at VTC, and Ms Ruth Macleod at the University of Glasgow for the
601 production of peptide arrays. Servier medical art, licensed under CC BY 4.0
602 https://creativecommons.org/licenses/by/4.0/, was used to create figure schematics. Funding for
603 this research includes AHA 19CDA34630036 (SJ), AHA 23PRE1010870 (MS), AHA
604 25POST1410066 (MR), NIH-F31HL170721 (MS), NIH-R215R21HL168614-02 (SJ), VT-Proof of
605 Concept (SJ), and the Seale Innovation Award (SJ). Medical Research Council grant
606 MR/y00364/1 (GSB). NIH HL120840, NIH HL137112.

607 **References**

608 1. Nedkoff L, Briffa T, Zemedikun D, Herrington S, Wright FL. Global Trends in
609 Atherosclerotic Cardiovascular Disease. *Clin Ther*. Nov 2023;45(11):1087-1091.
610 doi:10.1016/j.clinthera.2023.09.020
611 2. Maron DJ, Hochman JS, Reynolds HR, et al. Initial Invasive or Conservative Strategy for
612 Stable Coronary Disease. *N Engl J Med*. Apr 09 2020;382(15):1395-1407.
613 doi:10.1056/NEJMoa1915922
614 3. Déglise S, Bechelli C, Allagnat F. Vascular smooth muscle cells in intimal hyperplasia, an
615 update. *Front Physiol*. 2022;13:1081881. doi:10.3389/fphys.2022.1081881
616 4. Cornelissen A, Guo L, Fernandez R, et al. Endothelial Recovery in Bare Metal Stents and
617 Drug-Eluting Stents on a Single-Cell Level. *Arterioscler Thromb Vasc Biol*. Aug 2021;41(8):2277-
618 2292. doi:10.1161/ATVBAHA.121.316472
619 5. Bønaa KH, Mannsverk J, Wiseth R, et al. Drug-Eluting or Bare-Metal Stents for Coronary
620 Artery Disease. *N Engl J Med*. Sep 29 2016;375(13):1242-52. doi:10.1056/NEJMoa1607991
621 6. Goodenough DA, Goliger JA, Paul DL. Connexins, connexons, and intercellular
622 communication. *Annu Rev Biochem*. 1996;65:475-502.
623 doi:10.1146/annurev.bi.65.070196.002355
624 7. Gangoso E, Thirant C, Chneiweiss H, Medina JM, Tabernero A. A cell-penetrating peptide
625 based on the interaction between c-Src and connexin43 reverses glioma stem cell phenotype.
626 *Cell Death Dis*. Jan 23 2014;5:e1023. doi:10.1038/cddis.2013.560
627 8. Moorer MC, Hebert C, Tomlinson RE, Iyer SR, Chason M, Stains JP. Defective signaling,
628 osteoblastogenesis and bone remodeling in a mouse model of connexin 43 C-terminal truncation.
629 *J Cell Sci*. Feb 01 2017;130(3):531-540. doi:10.1242/jcs.197285
630 9. Langlois S, Cowan KN, Shao Q, Cowan BJ, Laird DW. The tumor-suppressive function of
631 Connexin43 in keratinocytes is mediated in part via interaction with caveolin-1. *Cancer Res*. May
632 15 2010;70(10):4222-32. doi:10.1158/0008-5472.CAN-09-3281
633 10. Gellhaus A, Dong X, Propson S, et al. Connexin43 interacts with NOV: a possible
634 mechanism for negative regulation of cell growth in choriocarcinoma cells. *J Biol Chem*. Aug 27
635 2004;279(35):36931-42. doi:10.1074/jbc.M404073200
636 11. Fu CT, Bechberger JF, Ozog MA, Perbal B, Naus CC. CCN3 (NOV) interacts with
637 connexin43 in C6 glioma cells: possible mechanism of connexin-mediated growth suppression. *J*
638 *Biol Chem*. Aug 27 2004;279(35):36943-50. doi:10.1074/jbc.M403952200
639 12. Strauss RE, Mezache L, Veeraraghavan R, Gourdie RG. The Cx43 Carboxyl-Terminal
640 Mimetic Peptide αCT1 Protects Endothelial Barrier Function in a ZO1 Binding-Competent
641 Manner. *Biomolecules*. Aug 12 2021;11(8)doi:10.3390/biom11081192
642 13. Smyth JW, Guo S, O'Rourke L, et al. Increased interaction between connexin43 and
643 microtubules is critical for glioblastoma stem-like cell maintenance and tumorigenicity. *bioRxiv*.
644 Jan 27 2024;doi:10.1101/2024.01.26.576347
645 14. Hong T, Hill CE. Restricted expression of the gap junctional protein connexin 43 in the
646 arterial system of the rat. *J Anat*. May 1998;192 (Pt 4)(Pt 4):583-93. doi:10.1046/j.1469-
647 7580.1998.19240583.x
648 15. Liao Y, Regan CP, Manabe I, et al. Smooth muscle-targeted knockout of connexin43
649 enhances neointimal formation in response to vascular injury. *Arterioscler Thromb Vasc Biol*. May
650 2007;27(5):1037-42. doi:10.1161/ATVBAHA.106.137182
651 16. Chadjichristos CE, Matter CM, Roth I, et al. Reduced connexin43 expression limits
652 neointima formation after balloon distension injury in hypercholesterolemic mice. *Circulation*. Jun
653 20 2006;113(24):2835-43. doi:10.1161/CIRCULATIONAHA.106.627703
654 17. Zhang A, Han Y, Wang B, Li S, Gan W. Beyond Gap Junction Channel Function: the
655 Expression of Cx43 Contributes to Aldosterone-Induced Mesangial Cell Proliferation via the
656 ERK1/2 and PKC Pathways. *Cell Physiol Biochem*. 2015;36(3):1210-22. doi:10.1159/000430291

657 18. Tittarelli A, Guerrero I, Tempio F, et al. Overexpression of connexin 43 reduces melanoma
658 proliferative and metastatic capacity. *Br J Cancer*. Jul 14 2015;113(2):259-67.
659 doi:10.1038/bjc.2015.162
660 19. Arshad M, Conzelmann C, Riaz MA, Noll T, Gündüz D. Inhibition of Cx43 attenuates
661 ERK1/2 activation, enhances the expression of Cav-1 and suppresses cell proliferation. *Int J Mol*
662 *Med*. Nov 2018;42(5):2811-2818. doi:10.3892/ijmm.2018.3828
663 20. Chadjichristos CE, Morel S, Derouette JP, et al. Targeting connexin 43 prevents platelet-
664 derived growth factor-BB-induced phenotypic change in porcine coronary artery smooth muscle
665 cells. *Circ Res*. Mar 28 2008;102(6):653-60. doi:10.1161/CIRCRESAHA.107.170472
666 21. Plenz G, Ko YS, Yeh HI, et al. Upregulation of connexin43 gap junctions between
667 neointimal smooth muscle cells. *Eur J Cell Biol*. Oct 2004;83(10):521-30. doi:10.1078/0171-9335-
668 00417
669 22. Yeh HI, Lupu F, Dupont E, Severs NJ. Upregulation of connexin43 gap junctions between
670 smooth muscle cells after balloon catheter injury in the rat carotid artery. *Arterioscler Thromb*
671 *Vasc Biol*. Nov 1997;17(11):3174-84. doi:10.1161/01.atv.17.11.3174
672 23. Sorgen PL, Duffy HS, Sahoo P, Coombs W, Delmar M, Spray DC. Structural changes in
673 the carboxyl terminus of the gap junction protein connexin43 indicates signaling between binding
674 domains for c-Src and zonula occludens-1. *J Biol Chem*. Dec 24 2004;279(52):54695-701.
675 doi:10.1074/jbc.M409552200
676 24. Johnstone SR, Kroncke BM, Straub AC, et al. MAPK phosphorylation of connexin 43
677 promotes binding of cyclin E and smooth muscle cell proliferation. *Circ Res*. Jul 6
678 2012;111(2):201-11. doi:10.1161/circresaha.112.272302
679 25. González-Sánchez A, Jaraíz-Rodríguez M, Domínguez-Prieto M, Herrero-González S,
680 Medina JM, Tabernero A. Connexin43 recruits PTEN and Csk to inhibit c-Src activity in glioma
681 cells and astrocytes. *Oncotarget*. Aug 02 2016;7(31):49819-49833.
682 doi:10.18632/oncotarget.10454
683 26. Solan JL, Marquez-Rosado L, Sorgen PL, Thornton PJ, Gafken PR, Lampe PD.
684 Phosphorylation at S365 is a gatekeeper event that changes the structure of Cx43 and prevents
685 down-regulation by PKC. *J Cell Biol*. Dec 17 2007;179(6):1301-9. doi:10.1083/jcb.200707060
686 27. Ohtsubo M, Theodoras AM, Schumacher J, Roberts JM, Pagano M. Human cyclin E, a
687 nuclear protein essential for the G1-to-S phase transition. *Mol Cell Biol*. May 1995;15(5):2612-24.
688 doi:10.1128/MCB.15.5.2612
689 28. George SJ, Wan S, Hu J, MacDonald R, Johnson JL, Baker AH. Sustained reduction of
690 vein graft neointima formation by ex vivo TIMP-3 gene therapy. *Circulation*. Sep 13 2011;124(11
691 Suppl):S135-42. doi:10.1161/CIRCULATIONAHA.110.012732
692 29. George SJ, Williams A, Newby AC. An essential role for platelet-derived growth factor in
693 neointima formation in human saphenous vein in vitro. *Atherosclerosis*. Feb 1996;120(1-2):227-
694 40. doi:10.1016/0021-9150(95)05717-x
695 30. Saxton RA, Sabatini DM. mTOR Signaling in Growth, Metabolism, and Disease. *Cell*. Mar
696 09 2017;168(6):960-976. doi:10.1016/j.cell.2017.02.004
697 31. Sedovy MW, Leng X, Iqbal F, et al. Preserving Endothelial Integrity in Human Saphenous
698 Veins during Preparation for Coronary Bypass Surgery. *J Vasc Res*. Jan 12 2024:1-9.
699 doi:10.1159/000535843
700 32. O'Sullivan M, Scott SD, McCarthy N, et al. Differential cyclin E expression in human in-
701 stent stenosis smooth muscle cells identifies targets for selective anti-restenosis therapy.
702 *Cardiovasc Res*. Dec 01 2003;60(3):673-83. doi:10.1016/j.cardiores.2003.09.018
703 33. Rhett JM, Calder BW, Fann SA, Bainbridge H, Gourdie RG, Yost MJ. Mechanism of action
704 of the anti-inflammatory connexin43 mimetic peptide JM2. *Am J Physiol Cell Physiol*. Sep 01
705 2017;313(3):C314-C326. doi:10.1152/ajpcell.00229.2016

706 34. Calder BW, Matthew Rhett J, Bainbridge H, Fann SA, Gourdie RG, Yost MJ. Inhibition of
707 connexin 43 hemichannel-mediated ATP release attenuates early inflammation during the foreign
708 body response. *Tissue Eng Part A*. Jun 2015;21(11-12):1752-62. doi:10.1089/ten.TEA.2014.0651
709 35. He D, Ma Z, Xue K, Li H. Juxtamembrane 2 mimic peptide competitively inhibits
710 mitochondrial trafficking and activates ROS-mediated apoptosis pathway to exert anti-tumor
711 effects. *Cell Death Dis*. Mar 24 2022;13(3):264. doi:10.1038/s41419-022-04639-6
712 36. Lampe PD, Kurata WE, Warn-Cramer BJ, Lau AF. Formation of a distinct connexin43
713 phosphoisoform in mitotic cells is dependent upon p34cdc2 kinase. *J Cell Sci*. Mar 1998;111 (Pt
714 6):833-41. doi:10.1242/jcs.111.6.833
715 37. Kanemitsu MY, Jiang W, Eckhart W. Cdc2-mediated phosphorylation of the gap junction
716 protein, connexin43, during mitosis. *Cell Growth Differ*. Jan 1998;9(1):13-21.
717 38. Cameron SJ, Malik S, Akaike M, et al. Regulation of epidermal growth factor-induced
718 connexin 43 gap junction communication by big mitogen-activated protein kinase1/ERK5 but not
719 ERK1/2 kinase activation. *J Biol Chem*. May 16 2003;278(20):18682-8.
720 doi:10.1074/jbc.M213283200
721 39. Doble BW, Dang X, Ping P, et al. Phosphorylation of serine 262 in the gap junction protein
722 connexin-43 regulates DNA synthesis in cell-cell contact forming cardiomyocytes. *J Cell Sci*. Jan
723 26 2004;117(Pt 3):507-14. doi:10.1242/jcs.00889
724 40. Jaraíz-Rodríguez M, Talaverón R, García-Vicente L, et al. Connexin43 peptide, TAT-
725 Cx43266-283, selectively targets glioma cells, impairs malignant growth, and enhances survival
726 in mouse models in vivo. *Neuro Oncol*. Apr 15 2020;22(4):493-504. doi:10.1093/neuonc/noz243
727 41. Jiang J, Hoagland D, Palatinus JA, et al. Interaction of α Carboxyl Terminus 1 Peptide
728 With the Connexin 43 Carboxyl Terminus Preserves Left Ventricular Function After Ischemia-
729 Reperfusion Injury. *J Am Heart Assoc*. Aug 20 2019;8(16):e012385.
730 doi:10.1161/JAHA.119.012385
731 42. King DR, Sedovy MW, Leng X, et al. Mechanisms of Connexin Regulating Peptides.
732 *International Journal of Molecular Sciences*. 2021;22(19)doi:10.3390/ijms
733 43. Jackman M, Kubota Y, den Elzen N, Hagting A, Pines J. Cyclin A- and cyclin E-Cdk
734 complexes shuttle between the nucleus and the cytoplasm. *Mol Biol Cell*. Mar 2002;13(3):1030-
735 45. doi:10.1091/mbc.01-07-0361
736 44. Moore JD, Yang J, Truant R, Kornbluth S. Nuclear import of Cdk/cyclin complexes:
737 identification of distinct mechanisms for import of Cdk2/cyclin E and Cdc2/cyclin B1. *J Cell Biol*.
738 Jan 25 1999;144(2):213-24. doi:10.1083/jcb.144.2.213
739 45. Gaulin JF, Fiset A, Fortier S, Faure RL. Characterization of Cdk2-cyclin E complexes in
740 plasma membrane and endosomes of liver parenchyma. Insulin-dependent regulation. *J Biol*
741 *Chem*. Jun 02 2000;275(22):16658-65. doi:10.1074/jbc.275.22.16658
742 46. Akiyama T, Ohuchi T, Sumida S, Matsumoto K, Toyoshima K. Phosphorylation of the
743 retinoblastoma protein by cdk2. *Proc Natl Acad Sci U S A*. Sep 01 1992;89(17):7900-4.
744 doi:10.1073/pnas.89.17.7900
745 47. O'Quinn MP, Palatinus JA, Harris BS, Hewett KW, Gourdie RG. A peptide mimetic of the
746 connexin43 carboxyl terminus reduces gap junction remodeling and induced arrhythmia following
747 ventricular injury. Research Support, N.I.H., Extramural Research Support, Non-U.S. Gov't.
748 *Circulation Research*. Mar 18 2011;108(6):704-15. doi:10.1161/circresaha.110.235747
749 48. Rhett JM, Jourdan J, Gourdie RG. Connexin 43 connexon to gap junction transition is
750 regulated by zonula occludens-1. *Mol Biol Cell*. May 2011;22(9):1516-28. doi:10.1091/mbc.E10-
751 06-0548
752 49. Ek-Vitorin JF, King TJ, Heyman NS, Lampe PD, Burt JM. Selectivity of connexin 43
753 channels is regulated through protein kinase C-dependent phosphorylation. *Circ Res*. Jun 23
754 2006;98(12):1498-505. doi:10.1161/01.RES.0000227572.45891.2c

755 50. Lampe PD, TenBroek EM, Burt JM, Kurata WE, Johnson RG, Lau AF. Phosphorylation of
756 connexin43 on serine368 by protein kinase C regulates gap junctional communication. *J Cell Biol*.
757 Jun 26 2000;149(7):1503-12. doi:10.1083/jcb.149.7.1503
758 51. Gaudino M, Benedetto U, Fremes S, et al. Radial-Artery or Saphenous-Vein Grafts in
759 Coronary-Artery Bypass Surgery. *N Engl J Med*. May 31 2018;378(22):2069-2077.
760 doi:10.1056/NEJMoa1716026
761 52. van der Meer J, Hillege HL, van Gilst WH, et al. A comparison of internal mammary artery
762 and saphenous vein grafts after coronary artery bypass surgery. No difference in 1-year occlusion
763 rates and clinical outcome. CABADAS Research Group of the Interuniversity Cardiology Institute
764 of The Netherlands. *Circulation*. Nov 1994;90(5):2367-74. doi:10.1161/01.cir.90.5.2367
765 53. Tector AJ, Schmahl TM, Janson B, Kallies JR, Johnson G. The internal mammary artery
766 graft. Its longevity after coronary bypass. *JAMA*. Nov 13 1981;246(19):2181-3.
767 54. Gaudino M, Bakaeen FG, Sandner S, et al. Expert Systematic Review on the Choice of
768 Conduits for Coronary Artery Bypass Grafting: Endorsed by the European Association for Cardio-
769 Thoracic Surgery (EACTS) and The Society of Thoracic Surgeons (STS). *Ann Thorac Surg*. Oct
770 2023;116(4):659-674. doi:10.1016/j.athoracsur.2023.06.010
771 55. Bonacquisti EE, Nguyen J. Connexin 43 (Cx43) in cancer: Implications for therapeutic
772 approaches via gap junctions. *Cancer Lett*. Feb 01 2019;442:439-444.
773 doi:10.1016/j.canlet.2018.10.043
774 56. Bolger GB, Baillie GS, Li X, et al. Scanning peptide array analyses identify overlapping
775 binding sites for the signalling scaffold proteins, beta-arrestin and RACK1, in cAMP-specific
776 phosphodiesterase PDE4D5. *Biochem J*. Aug 15 2006;398(1):23-36. doi:10.1042/BJ20060423
777 57. Futaki S, Ohashi W, Suzuki T, et al. Stearylated arginine-rich peptides: a new class of
778 transfection systems. *Bioconjug Chem*. Nov-Dec 2001;12(6):1005-11. doi:10.1021/bc015508l
779 58. Johnstone SR, Ross J, Rizzo MJ, et al. Oxidized phospholipid species promote in vivo
780 differential cx43 phosphorylation and vascular smooth muscle cell proliferation. *Am J Pathol*. Aug
781 2009;175(2):916-24. doi:ajpath.2009.090160 [pii]
782 10.2353/ajpath.2009.090160
783 59. Yang Y, Delalio LJ, Best AK, et al. Endothelial Pannexin 1 Channels Control Inflammation
784 by Regulating Intracellular Calcium. *J Immunol*. Jun 2020;204(11):2995-3007.
785 doi:10.4049/jimmunol.1901089

Figure Legends:

Figure 1: PDGF-β induces new intima in human saphenous veins in vitro, associated with an increase in Cx43 and proliferation markers. Schematic of human saphenous vein tissue harvesting. Excess saphenous veins, used for coronary artery bypass graft, were dissected open with the luminal side up, cut free from valves and sutured vessels, and sequential sections were plated for testing. Media containing 2% serum was compared with samples treated with 50 ng PDGF, which was changed daily (**A**). Tissues were sectioned and stained for H&E, Tgln (orange), Cx43 (magenta), Cx43pS279 (red), and cyclin E (white) (**B**). n=3-5 samples used for staining. * indicates luminal side of the vessel, arrow indicates regions of new intima that were detected in tissues, scale bar is 50 μM.

Figure 2: Design of the CycliCx peptide using peptide arrays demonstrates cyclin E binding regions on the phosphorylated Cx43CT. Schematic showing the design for peptide arrays for using a sequence corresponding to the 180 a.a. Cx43-CT (**A**). Sequential 25 a.a. sequences were printed to nitrocellulose; consecutive sequences were overlapped by 5 a.a. (**A**). Eluted fractions from GST columns for cyclin E-GST proteins expressed in bacteria, expression shown by western blotting (anti-cyclin E, upper blot) and coomassie staining (lower gel, **B**). Peptide arrays with $Cx43CT^{WT}$ (red box) or MAPK phosphorylated Cx43-S255/262/279/282 (MK4) substitutions with either alanine ($Cx43^{MK4A}$, blue), aspartate ($Cx43^{MK4D}$, green), or native phosphor-serine ($Cx43^{MK4pS}$, orange) were bound by cyclin E proteins and detect with anti-cyclin E (**C**). Potential binding sites highlighted by red circles (**C**) and cyclin E arrays aligned with UV imaging of total peptide (**D**). Three potential binding sequence regions in $Cx43^{MK4D}$ and $Cx43^{MK4pS}$ are underlined (**E**). Analysis of the first three 25 a.a. binding sequences in Cx43 CT spanning Cx43 a.a. 236-300 shows phospho-specific binding only within Cx43 a.a. 236-285 (**F**), locations shown in schematic (**G**). Truncation mutation peptide array across Cx43 a.a. 255-272 used to define the minimum binding region (**H**). A schematic showing the location of the binding region and selected adjacent region used as an Off-Target (OT) peptide (**I**). The final design of the CycliCx peptide incorporating an N-terminal stearyl group (**J**)

Figure 3: CycliCx Peptide alters Cx43 expression and interactions with cyclin E.

CASMC treated with PDGF (PD, 50 ng/ mL) alone or in combination with OT peptide or CycliCx (30 μM) for 16 hr. Western blots were performed for total-ERK (tERK), phosphorylated-ERK (pERK phosphor ERK Thr202/Tyr204), and ratio of pERK: pERK calculated (n=6) (**A**), for total Cx43 and PKC-phosphorylated Cx43 (Cx43-PKC, pS368) (n=6), and alterations in expression from not treated (NT) calculated (**B**). Distribution and frequency of Cx43 GJ punctates (magenta) in treated CASMC (TGLN, Green) were captured by confocal microscopy, and differences in gap junction punctates/ cell were measured using NIS-elements software (n=3) (**C**). Cell plasma membrane protein biotinylation western blots for membrane-bound Cx43 (streptavidin eluted) compared to cytosolic (non-biotin bound) proteins (n=3) (**D**). Cell-to-cell communication through gap junctions was assessed by lucifer yellow dye transfer (green) in scrape-wounded monolayers of CASMC after treatment with PDGF or PDGF plus OT/ CycliCx peptide (n=6). Scrape load dye transfer (SLDT) of lucifer yellow (green) permeability was used to measure gap junction dye transfer, area of dye normalized to length, with co-loading of high molecular weight dextran (magenta) used to determine non-gap junction dye area (n=6) (**E**) Co-immunoprecipitation western blots were performed to assess Cx43-cyclin E binding in CASMC following peptide

treatment (IP cyclin E, WB Cx43) (n=4), with loading control western blot for Cx43 or cyclin E proteins (**F**). Sample loading for western blots was normalized to total protein or β-tubulin expression, and comparisons were made to NT cells (**A, B, D, F**). One-way ANOVA with multiple comparison test performed, P<0.05 is significant.

Figure 4: Transcriptomics reveals that the CycliCx peptide arrests cell cycle progression at G1/S phase transition. 5-ethynyl-2'-deoxyuridine (EDU) proliferation assay in human coronary artery smooth muscle cells (CASMC; **A**). Schematic showing the design for bulk RNA sequencing and group combinations for analysis (**B**). Principal component analysis (PCA) of 'DESeq2' normalized and $\log_2$ transformed counts (**C**). Volcano plots of 'DESeq2' differentially expressed genes (DEGs) identified with $|\log_2(\text{Fold Change (FC)})| > 0$ and an adjusted p-value (padj) < 0.05 for indicated group comparisons (**D**). Venn diagram of the total number of identified DEGs unique to and shared by the PDGF-β (PD) + Off Target Peptide (OT) and PD + CycliCx peptide treatment groups when compared to PD treatment alone (**E**). Top 10 pathways by padj from Gene Ontology (GO) Biological Process pathway analysis ranked by gene ratio (left panel shows top 10 upregulated pathways in PD vs no treatment (NT) and right panel shows top 10 downregulated pathways in PD + CycliCx vs PD + OT; **F**). Heatmap of between replicate 'DESeq2' normalized gene expression z-scores for PD + CycliCx vs PD + OT DEGs from the significantly enriched GO pathway GO:0000082: 'cell cycle G1/S phase transition (**G**). 'DESeq2' normalized gene counts in selected genes (**H**). N = 3-4 per group. Data displayed as mean ± SEM. P-values calculated by Tukey's multiple comparison testing after one-way ANOVA.

Figure 5: CycliCx peptide limits neointima formation in mouse and human blood vessels

H&E staining of mouse carotids following 14 days of sham surgery (no ligation) or ligation with either pluronic gel, pluronic+OT peptide or pluronic+CycliCx pep (200 μM). Measure of media area, neointima area, and ratio of neointima to media. Kruskal-Wallis multiple comparison test, N=12 (9 male, 3 female). H&E staining of human saphenous veins treated with PDGF+OT pep or PDGF+CycliCx for 14 days. Tgln staining of human saphenous veins treated with PDGF+OT pep or PDGF+CycliCx for 14 days. T-test, n=5.

Supplemental Figure Legends:

Supplemental Figure 1: Human saphenous vein H&E staining comparison. Representative images of H&E-stained human saphenous veins for no treatment (NT), PDGF, PDGF+ OT peptide, and PDGF+ CycliCx. * indicates luminal side of the vessel, arrow indicates regions of new intima that were detected in tissues, scale bar is 50 μM. N=5.

Supplemental Figure 2: Human saphenous vein smooth muscle cell transgelin staining. Representative images of anti-TGLN stained human saphenous veins for no treatment (NT), PDGF, PDGF+ OT peptide, PDGF+ CycliCx. Measurement of the leading edge (16pt) TGLN staining, averaged n=5-6 measures per tissue. * indicates luminal side of the vessel, arrow indicates regions of new intima that were detected in tissues, scale bar is 50 μM. N=5. Mann-Whitney tests were used for NT:PDGF, PD+OT peptide:PDGF+CycliCx, and Kruskal-Wallis multiple comparison test of all values. Exact P values shown.

Supplemental Figure 3: Human saphenous vein Cx43 staining comparison. Representative images of anti-Cx43 stained human saphenous veins for no treatment (NT), PDGF, PDGF+ OT peptide, and PDGF+ CycliCx. * indicates luminal side of the

vessel, arrow indicates regions of new intima that were detected in tissues, scale bar is 50 μM. N=3.

Supplemental Figure 4: Human saphenous vein Cx43-pS279 staining comparison. Representative images of anti-Cx43-pS279 stained human saphenous veins for no treatment (NT), PDGF, PDGF+ OT peptide, and PDGF+ CycliCx. * indicates luminal side of the vessel, arrow indicates regions of new intima that were detected in tissues, scale bar is 50 μM. N=3.

Supplemental Figure 5: Human saphenous vein cyclin E staining comparison. Representative images of anti-cyclin E1-stained human saphenous veins for no treatment (NT), PDGF, PDGF+ OT peptide, and PDGF+ CycliCx. * indicates luminal side of the vessel, arrow indicates regions of new intima that were detected in tissues, scale bar is 50 μM. N=3.

Supplemental Figure 6: Identification of active cyclin E binding sites on Cx43.

In **A**, Single Alanine amino acid substitutions for Cx43 sequences Seq1 Cx43 a.a. 235-260 (white), Seq 2 Cx43 a.a. 254-279 (green), Seq 3 Cx43 a.a. 276-301 (black). Full length sequences contain either native phosphoserine (ps) or aspartate (D). The first four spots contain a full sequence with either serines (S), alanines (A), pS, or D, and were used as representative images for **Figure 2**. In **A**, arrays were imaged with UV (total peptides, left), then probed with anti-cyclin E, and detected with a secondary antibody before development by chemiluminescence onto x-ray film (right). In **B**, truncation mutation arrays were performed on identified sequences (see **supplemental list** for sequences), detected with anti-cyclin E antibodies (top), and imaged with UV and Coomassie (total peptides). In **C**, alignments show the minimum binding sites identified across the Cx43-MAPK binding region (top, Sequence 2) and at a distant site (bottom, Sequence 1). Flow cytometry of stearate-linked peptides targeting Sequence 1 and Sequence 2 were generated and incubated with SMC (30 μM) in the presence of PDGF and EDU for proliferation (**D**). Sequence 1 reduced cell numbers, indicating cell death. Final design of peptide sequences based on binding characteristics seen by truncation arrays for CycliCx peptide (binding), and Off-Target peptide (OT peptide, non-binding), approximate charge, and molecular weight not including stearate group (**E**).

Supplemental Figure 7: Full blots for ERK measurements. CASMC were treated with PDGF-β (50 ng/ mL) alone or in combination with OT peptide or CycliCx (30 μM) for 16 hr. Western blots were performed for total ERK (tERK, p42/p44), phosphorylated ERK (pERK phosphor- p42/p44 Thr202/Tyr204) and ratio of pERK: pERK calculated (n=6). Total protein blots highlight equal loading of samples. Sample loading was normalized to total protein expression, and differences in expression were measured against non-treated cells. One-way ANOVA with multiple comparison test was performed, $P<0.05$ is significant. Orange box indicates blots used in **Figure 3**.

Supplemental Figure 8: Full blots for Cx43 measurements: CASMC were treated with PDG-β (50 ng/ mL) alone or in combination with OT peptide or CycliCx (30 μM) for 16 hr. Western blots were performed for Total Cx43 and Cx43 (n=3), Cx43-PKC Cx43-pS368) (n=6). Sample loading was normalized to total protein expression, and differences in expression measured against NT cells. One way ANOVA with multiple comparison test performed, $P<0.05$ is significant. Orange box indicates blots used in **Figure 3**.

Supplemental Figure 9: CycliCx alters Cx43 phosphorylation expression from 3 hours post-treatment. CASMC were treated with CycliCx (30 μM) and harvested every hour up until 5 hr. Expression of total Cx43 and Cx43-PKC (Cx43-pS368) was measured. Data show a trend towards an increase in Cx43-PKC from approximately 3 hr post-treatment (n=2).

Supplemental Figure 10: IF of Cx43 expression in SMC following PDGF and peptide treatments. Cells were treated for 16 hr with PDGF-β or PDGF-β with OT pep or CycliCx (30 μm). An n=3 images were taken per experiment (n=3), and results were averaged in the analysis. Highlighted boxes indicate images used in **Figure 3**.

Supplemental Figure 11: Full blots for plasma membrane protein biotinylation in CASMC. CASMC were treated with PDGF-β (50 ng/ mL) alone or in combination with OT peptide or CycliCx (30 μM) for 16 hr. Western blots for Cx43 show plasma membrane-bound proteins (streptavidin eluted, upper blots) compared to cytosolic (non-biotin bound, Lower) proteins (n=3). Orange boxes indicate blots used in **Figure 3**.

Supplemental Figure 12: IF of scrape load dye transfer in SMC following PDGF-β and peptide treatments. CASMC were scraped using a scalpel, followed by the addition of lucifer yellow (green) and Dextran (magenta). For each treatment group (NT, PDGF-β, PDGF-β + OT peptide, and PDGF-β + CycliCx) n=6 biological replicas were used (**A**). NIE image processing software was used to define the dye transfer area (**B**) and calculate the area of lucifer yellow gap junction dye spread minus the area of dextran used to detect scrape-injured cells (**C**). Both total dye area and dye area per scrape length were graphed (**D**). One way ANOVA with multiple comparison test performed, $P<0.05$ is significant.

Supplemental Figure 13: Full Co-immunoprecipitation western blots for Cx43 and cyclin E. CASMC were treated with PDGF-β (50 ng/ mL) alone or in combination with OT peptide or CycliCx (30 μM) for 16 hr. Blots show cyclin E co-immunoprecipitation with Cx43 detected by western blot (n=3). Control loading blots for Cx43, cyclin E, β- β-tubulin, and total protein. N=4, One-way ANOVA with multiple comparison test performed, $P<0.05$ is significant. (Orange boxes indicate blots used in Figure 3)

Supplemental Figure 14: SMC EDU proliferation flow cytometry histogram data. Histogram replicates for SMC EDU fluorescence gating for cells treated with PDGF-β, PDGF-β+OT pep, and PDGF-β+CycliCx. N=6 replicates

Supplemental Figure 15: Bulk RNA sequencing quality control, correlation, and clustering. G/C and A/T content distribution along sequence reads for individual replicates in the PDGF-β (PD) group (**A**). Pearson's correlation coefficient matrix of FPKM normalized gene counts before (top panel) and after (bottom panel) removal of the outlying PD replicate (**B**). Heatmap of between replicate FPKM normalized gene expression z-scores with hierarchical clustering (**C**). N = 3-4 per group. Con = no treatment control group; Pep4 = off-target (OT) control peptide; Pep5 = CycliCx peptide.

Supplemental Figure 16: CycliCx peptide blunts mitotic gene pathways. Heatmaps of between replicate 'DESeq2' normalized gene expression z-scores for PDGF-β (PD) + CycliCx vs PD + Off Target Peptide (OT Pep) differentially expressed genes (DEGs) from the significantly enriched GO pathways GO:0044839: 'cell cycle G2/M phase transition (**A**), and GO:0140014 'mitotic nuclear division' (**B**). N = 3-4 per group. NT = No Treatment control group.

Supplemental Figure 17: CycliCx peptide alters the expression of critical cell cycle regulatory genes. 'DESeq2' normalized gene counts in selected genes that regulate early G1 phase progression (**A**), G1/S phase transition (**B**), and G2/M phase transition (**C**). Separated based on CycliCx regulation. N = 3-4 per group. Data displayed as mean ± SEM. NT = No Treatment control group; PD = PDGF-β; OT = Off Target peptide.

Supplemental Figure 18: Gene expression of gap junction proteins and PDGF regulators and transcription targets. 'DESeq2' normalized gene counts in selected gap junction genes (**A**), G1/S phase transition (**B**), and in PDGF regulatory kinases (Erk1/2) and non-cell cycle PDGF transcription targets (**C**). N = 3-4 per group. Data displayed as mean ± SEM. NT = No Treatment control group; PD = PDGF-β; OT = Off Target peptide.

Supplemental Figure 19: CycliCx peptide blunts the expression of smooth muscle contractile genes. 'DESeq2' normalized gene counts in selected vascular smooth muscle cell contractile genes. N = 3-4 per group. Data displayed as mean ± SEM. NT = No Treatment control group; PD = PDGF-β; OT = Off Target peptide.

Supplemental Figure 20: Mouse ligation neointima measurements. H&E staining of mouse carotids following 14 days of sham surgery (no ligation) or ligation with either pluronic gel, pluronic plus OT peptide or pluronic CycliCx peptide. Measure of media area, neointima area and ration of neointima to media. Highlighted images are used as a representative in **Figure 5**. Kruskal-Wallis multiple comparison test, N=12 (9 male, 3 female). * indicates luminal side of the vessel, arrow indicates regions of new intima that were detected in tissues, scale bar is 100 μM.

Supplemental Table 1: Key Resource Table

REAGENT or RESOURCE	SOURCE	IDENTIFIER
Antibodies (IF/ WB/ CO-IP)		
Cx43 (WB/ CO-IP)	Millipore Sigma	C6219 RRID:AB_476857
Cx43 (IF, Rabbit)	Millipore Sigma	HPA035097 UNSPSC:12352203
Cx43 (WB/ CO-IP)	Millipore Sigma	C8093 RRID:AB_259085
Phospho-Cx43 (pSer368) (WB)	Millipore Sigma	SAB4504371
Phospho-Cx43 (pSer 279/282) 0.19 g/mL (IF)	custom antibody Source Dr. Paul Lampe,	Reference PMID: 22652908
Cyclin E1, CCNE1-HE12 (IF, Mouse)	Cell Signaling Technologies	4129
Cyclin E (CCNE1) (IF, WB, Rabbit)	Millipore Sigma	SAB1400044
p44/42 MAPK (Erk1/2) (137F5, Rabbit)	Cell Signaling Technologies	4695
Phospho-p44/42 MAPK (Erk1/2) (Thr202/Tyr204) (D13.14.4E) XP®, Rabbit	Cell Signaling Technologies	4370
β-Tubulin (WB, Mouse)	DSHB	E7 RRID:AB_2315513
Transgelin (IF, Goat)	Abcam	ab10135
IRDye® 800CW, Donkey Anti-Rabbit	LI-COR Biosciences	926-32213 RRID:AB_621848
IRDye® 800CW, Donkey Anti-Mouse	LI-COR Biosciences	926-32212, RRID:AB_621847

IRDy(R) 680RD Donkey anti-Rabbit	LI-COR Biosciences	926-68073 RRID:AB_10954442
IRDye 680RD Donkey anti-Mouse	LI-COR Biosciences	926-68072 RRID:AB_10953628
IRDye®800CW Streptavidin	LI-COR Biosciences	926-32230
Chemicals and Reagents		
Gibco™ M231 media	ThermoFisher Scientific	M-231-500
VWR Life Science Seradigm Premium Grade Fetal Bovine Serum	VWR Life Science	97068-085
Smooth muscle growth supplement (SMGS)	ThermoFisher Scientific	S00725
Trypsin-EDTA (0.5%), no phenol red	ThermoFisher Scientific	15400-054
Gibco™ M231 media	ThermoFisher Scientific	M-231-500
DPBS (1X), no calcium, no magnesium	ATCC	30-2200
Recombinant PDGF-bb	Millipore	01-305
Ethylene glycol-bis(2-aminoethylether)-N,N,N′,N′-tetraacetic acid	Sigma-Aldrich	E4378
Protease Inhibitor Cocktail	Millipore Sigma	P8340
phosphatase Inhibitor Cocktail 2	Millipore Sigma	P5726
phosphatase Inhibitor Cocktail 3	Millipore Sigma	P0044
RNeasy kit	Qiagen	74004
Odyssey Blocking Buffer (PBS)	LI-COR Biosciences	927-40000

Dynabeads™ M-280 Streptavidin	ThermoFisher Scientific	11205D
EZ-Link™ Sulfo-NHS-LC-Biotin	ThermoFisher Scientific	21335
5-ethynyl-2'deoxyuridine (EDU) Flow cytometry kitt-488 (	ThermoFisher Scientific	C10425
Ethiqa XR 1.3 mg/mL	Covetrus	072117
Isoflurane	Covetrus	029405
Pluronic F127	Millipore Sigma	P2443
CycliCx Peptide: stearate-LDPSKDCGDPKYAY	ThermoFisher custom peptide synthesis services	Custom
OT Peptide: stearate-AYFNGCSSPTAPLDP	ThermoFisher custom peptide synthesis services	Custom
Commercial Assays		
Pierce™ BCA Protein Assay Kit	ThermoFisher Scientific	23225
REVERT™ Total Protein Stain for immunoblot Normalization	LI-COR Biosciences	926-11010
Experimental Models: Cell lines and Mice		
CASMC: primary human SMC	ATCC	PCS-100-02
CASMC: primary human SMC	Lonza	CC-2583
CASMC: primary human SMC	Thermo Fisher Scientific	C0175C
C57BL/6J mice	Jackson Laboratory	000664

Key:
IF – Immunofluorescence

WB – Western blot
Co-IP co-immunoprecipitation

Supplemental List Cx43CT Truncation Mutation array
Full sequence
QGPLGVKDRVKGRSDPYHATTGPLSPSKDCGSPKYAYFNGCSSPTAPLSPMSPPGYKLVTGDRNNSSCRN

Arrays

(1)

1. Q G P L G V K D R V K G R S D P Y H A T T G P L pS
2. Q G P L G V K D R V K G R S D P Y H A T T G P L S
3. Q G P L G V K D R V K G R S D P Y H A T T G P L A
4. G P L G V K D R V K G R S D P Y H A T T G P L pS
5. P L G V K D R V K G R S D P Y H A T T G P L pS
6. L G V K D R V K G R S D P Y H A T T G P L pS
7. G V K D R V K G R S D P Y H A T T G P L pS
8. V K D R V K G R S D P Y H A T T G P L pS
9. K D R V K G R S D P Y H A T T G P L pS
10. D R V K G R S D P Y H A T T G P L pS
11. R V K G R S D P Y H A T T G P L pS
12. V K G R S D P Y H A T T G P L pS
13. K G R S D P Y H A T T G P L pS
14. G R S D P Y H A T T G P L pS
15. R S D P Y H A T T G P L pS
16. S D P Y H A T T G P L pS
17. D P Y H A T T G P L pS
18. P Y H A T T G P L pS
19. Y H A T T G P L pS
20. H A T T G P L pS
21. A T T G P L pS
22. T T G P L pS
23. T G P L pS
24. P L pS
25. L pS
26. pS
27. .space

(2)

1. Q G P L G V K D R V K G R S D P Y H A T T G P L pS
2. Q G P L G V K D R V K G R S D P Y H A T T G P L S
3. Q G P L G V K D R V K G R S D P Y H A T T G P L A
4. Q G P L G V K D R V K G R S D P Y H A T T G P L
5. Q G P L G V K D R V K G R S D P Y H A T T G P
6. Q G P L G V K D R V K G R S D P Y H A T T G
7. Q G P L G V K D R V K G R S D P Y H A T T
8. Q G P L G V K D R V K G R S D P Y H A T
9. Q G P L G V K D R V K G R S D P Y H A
10. Q G P L G V K D R V K G R S D P Y H
11. Q G P L G V K D R V K G R S D P Y
12. Q G P L G V K D R V K G R S D P
13. Q G P L G V K D R V K G R S D
14. Q G P L G V K D R V K G R S
15. Q G P L G V K D R V K G R
16. Q G P L G V K D R V K G
17. Q G P L G V K D R V K
18. Q G P L G V K D R V
19. Q G P L G V K D R
20. Q G P L G V K D
21. Q G P L G V K
22. Q G P L G V
23. Q G P L G
24. Q G P L
25. Q G P
26. Q G
27. Q
28. .space

(3)pS

1. P S K D C G pS P K Y A Y F N G C S S P T A P L pS P
2. P S K D C G S P K Y A Y F N G C S S P T A P L S P
3. P S K D C G A P K Y A Y F N G C S S P T A P L A P
4. S K D C G pS P K Y A Y F N G C S S P T A P L pS P
5. K D C G pS P K Y A Y F N G C S S P T A P L pS P
6. D C G pS P K Y A Y F N G C S S P T A P L pS P
7. C G pS P K Y A Y F N G C S S P T A P L pS P

8. G pS P K Y A Y F N G C S S P T A P L pS P
9. pS P K Y A Y F N G C S S P T A P L pS P
10. P K Y A Y F N G C S S P T A P L pS P
11. K Y A Y F N G C S S P T A P L pS P
12. Y A Y F N G C S S P T A P L pS P
13. A Y F N G C S S P T A P L pS P
14. Y F N G C S S P T A P L pS P
15. F N G C S S P T A P L pS P
16. N G C S S P T A P L pS P
17. G C S S P T A P L pS P
18. C S S P T A P L pS P
19. S S P T A P L pS P
20. S P T A P L pS P
21. P T A P L pS P
22. A P L pS P
23. P L pS P
24. L pS P
25. pS P
26. P
27. .space

(4)pS

1. P S K D C G pS P K Y A Y F N G C S S P T A P L pS P
2. P S K D C G S P K Y A Y F N G C S S P T A P L S P
3. P S K D C G A P K Y A Y F N G C S S P T A P L A P
4. P S K D C G pS P K Y A Y F N G C S S P T A P L pS
5. P S K D C G pS P K Y A Y F N G C S S P T A P L
6. P S K D C G pS P K Y A Y F N G C S S P T A P
7. P S K D C G pS P K Y A Y F N G C S S P T A
8. P S K D C G pS P K Y A Y F N G C S S P T
9. P S K D C G pS P K Y A Y F N G C S S P
10. P S K D C G pS P K Y A Y F N G C S S
11. P S K D C G pS P K Y A Y F N G C S
12. P S K D C G pS P K Y A Y F N G C
13. P S K D C G pS P K Y A Y F N G
14. P S K D C G pS P K Y A Y F N
15. P S K D C G pS P K Y A Y F
16. P S K D C G pS P K Y A Y
17. P S K D C G pS P K Y A
18. P S K D C G pS P K Y
19. P S K D C G pS P K
20. P S K D C G pS P
21. P S K D C G pS
22. P S K D C G
23. P S K D C
24. P S K D
25. P S K
26. P S
27. P
28. .space

(5)

1. A P L pS P M pS P P G Y K L V T G D R N N S S C R N
2. A P L S P M S P P G Y K L V T G D R N N S S C R N
3. A P L A P M A P P G Y K L V T G D R N N S S C R N
4. P L pS P M pS P P G Y K L V T G D R N N S S C R N
5. P L pS P M pS P P G Y K L V T G D R N N S S C R N
6. pS P M pS P P G Y K L V T G D R N N S S C R N
7. P M pS P P G Y K L V T G D R N N S S C R N
8. M pS P P G Y K L V T G D R N N S S C R N
9. pS P P G Y K L V T G D R N N S S C R N
10. P P G Y K L V T G D R N N S S C R N
11. P G Y K L V T G D R N N S S C R N
12. G Y K L V T G D R N N S S C R N
13. Y K L V T G D R N N S S C R N
14. K L V T G D R N N S S C R N
15. L V T G D R N N S S C R N
16. V T G D R N N S S C R N
17. T G D R N N S S C R N
18. G D R N N S S C R N
19. R N N S S C R N
20. N N S S C R N
21. N S S C R N

22. S S C R N
23. S C R N
24. C R N
25. R N
26. N
27. .space

(6) pS

1. A P L pS P M pS P P G Y K L V T G D R N N S S C R N
2. A P L S P M S P P G Y K L V T G D R N N S S C R N
3. A P L A P M A P P G Y K L V T G D R N N S S C R N
4. A P L pS P M pS P P G Y K L V T G D R N N S S C R
5. A P L pS P M pS P P G Y K L V T G D R N N S S C
6. A P L pS P M pS P P G Y K L V T G D R N N S S
7. A P L pS P M pS P P G Y K L V T G D R N N S
8. A P L pS P M pS P P G Y K L V T G D R N N
9. A P L pS P M pS P P G Y K L V T G D R N
10. A P L pS P M pS P P G Y K L V T G D R
11. A P L pS P M pS P P G Y K L V T G D
12. A P L pS P M pS P P G Y K L V T G
13. A P L pS P M pS P P G Y K L V T
14. A P L pS P M pS P P G Y K L V
15. A P L pS P M pS P P G Y K L
16. A P L pS P M pS P P G Y K
17. A P L pS P M pS P P G Y
18. A P L pS P M pS P P G
19. A P L pS P M pS P P
20. A P L pS P M pS P
21. A P L pS P M pS
22. A P L pS P M
23. A P L pS P
24. A P L pS
25. A P L
26. A P
27. A
28. .space

(7) pS

1. pS P S K D C G pS P K Y A Y F N G C S S P T A P L pS P M pS
2. S P S K D C G S P K Y A Y F N G C S S P T A P L S P M S
3. A P S K D C G A P K Y A Y F N G C S S P T A P L A P M A
4. P S K D C G pS P K Y A Y F N G C S S P T A P L pS P M pS
5. S K D C G pS P K Y A Y F N G C S S P T A P L pS P M pS
6. K D C G pS P K Y A Y F N G C S S P T A P L pS P M pS
7. D C G pS P K Y A Y F N G C S S P T A P L pS P M pS
8. C G pS P K Y A Y F N G C S S P T A P L pS P M pS
9. G pS P K Y A Y F N G C S S P T A P L pS P M pS
10. pS P K Y A Y F N G C S S P T A P L pS P M pS
11. P K Y A Y F N G C S S P T A P L pS P M pS
12. K Y A Y F N G C S S P T A P L pS P M pS
13. Y A Y F N G C S S P T A P L pS P M pS
14. A Y F N G C S S P T A P L pS P M pS
15. Y F N G C S S P T A P L pS P M pS
16. F N G C S S P T A P L pS P M pS
17. N G C S S P T A P L pS P M pS
18. G C S S P T A P L pS P M pS
19. C S S P T A P L pS P M pS
20. S S P T A P L pS P M pS
21. S P T A P L pS P M pS
22. P T A P L pS P M pS
23. T A P L pS P M pS
24. A P L pS P M pS
25. P L pS P M pS
26. L pS P M pS
27. pS P M pS
28. P M pS
29. M pS
30. pS
31. .space

(8) pS

1. pS P S K D C G pS P K Y A Y F N G C S S P T A P L pS P M pS

2. S P S K D C G S P K Y A Y F N G C S S P T A P L S P M S
3. A P S K D C G A P K Y A Y F N G C S S P T A P L A P M A
4. pS P S K D C G pS P K Y A Y F N G C S S P T A P L pS P M
5. pS P S K D C G pS P K Y A Y F N G C S S P T A P L pS P
6. pS P S K D C G pS P K Y A Y F N G C S S P T A P L pS
7. pS P S K D C G pS P K Y A Y F N G C S S P T A P L
8. pS P S K D C G pS P K Y A Y F N G C S S P T A P
9. pS P S K D C G pS P K Y A Y F N G C S S P T A
10. pS P S K D C G pS P K Y A Y F N G C S S P T
11. pS P S K D C G pS P K Y A Y F N G C S S P
12. pS P S K D C G pS P K Y A Y F N G C S S
13. pS P S K D C G pS P K Y A Y F N G C S
14. pS P S K D C G pS P K Y A Y F N G C
15. pS P S K D C G pS P K Y A Y F N G
16. pS P S K D C G pS P K Y A Y F N
17. pS P S K D C G pS P K Y A Y F
18. pS P S K D C G pS P K Y A Y
19. pS P S K D C G pS P K Y A
20. pS P S K D C G pS P K Y
21. pS P S K D C G pS P K
22. pS P S K D C G pS P
23. pS P S K D C G pS
24. pS P S K D C G
25. pS P S K D C
26. pS P S K D
27. pS P S K
28. pS P S
29. pS P
30. pS
31. sp

(9) D

1. Q G P L G V K D R V K G R S D P Y H A T T G P L D
2. Q G P L G V K D R V K G R S D P Y H A T T G P L S
3. Q G P L G V K D R V K G R S D P Y H A T T G P L A
4. G P L G V K D R V K G R S D P Y H A T T G P L D
5. P L G V K D R V K G R S D P Y H A T T G P L D
6. L G V K D R V K G R S D P Y H A T T G P L D
7. G V K D R V K G R S D P Y H A T T G P L D
8. V K D R V K G R S D P Y H A T T G P L D
9. K D R V K G R S D P Y H A T T G P L D
10. D R V K G R S D P Y H A T T G P L D
11. R V K G R S D P Y H A T T G P L D
12. V K G R S D P Y H A T T G P L D
13. K G R S D P Y H A T T G P L D
14. G R S D P Y H A T T G P L D
15. R S D P Y H A T T G P L D
16. S D P Y H A T T G P L D
17. D P Y H A T T G P L D
18. P Y H A T T G P L D
19. Y H A T T G P L D
20. H A T T G P L D
21. A T T G P L D
22. T T G P L D
23. T G P L D
24. P L D
25. L D
26. D
27. .space

(10)

1. Q G P L G V K D R V K G R S D P Y H A T T G P L D
2. Q G P L G V K D R V K G R S D P Y H A T T G P L S
3. Q G P L G V K D R V K G R S D P Y H A T T G P L A
4. Q G P L G V K D R V K G R S D P Y H A T T G P L
5. Q G P L G V K D R V K G R S D P Y H A T T G P
6. Q G P L G V K D R V K G R S D P Y H A T T G
7. Q G P L G V K D R V K G R S D P Y H A T T
8. Q G P L G V K D R V K G R S D P Y H A T
9. Q G P L G V K D R V K G R S D P Y H A
10. Q G P L G V K D R V K G R S D P Y H

11. Q G P L G V K D R V K G R S D P Y
12. Q G P L G V K D R V K G R S D P
13. Q G P L G V K D R V K G R S D
14. Q G P L G V K D R V K G R S
15. Q G P L G V K D R V K G R
16. Q G P L G V K D R V K G
17. Q G P L G V K D R V K
18. Q G P L G V K D R V
19. Q G P L G V K D R
20. Q G P L G V K D
21. Q G P L G V K
22. Q G P L G V
23. Q G P L G
24. Q G P L
25. Q G P
26. Q G
27. Q
28. .space;

(11) D

1. P S K D C G D P K Y A Y F N G C S S P T A P L D P
2. P S K D C G S P K Y A Y F N G C S S P T A P L S P
3. P S K D C G A P K Y A Y F N G C S S P T A P L A P
4. S K D C G D P K Y A Y F N G C S S P T A P L D P
5. K D C G D P K Y A Y F N G C S S P T A P L D P
6. D C G D P K Y A Y F N G C S S P T A P L D P
7. C G D P K Y A Y F N G C S S P T A P L D P
8. G D P K Y A Y F N G C S S P T A P L D P
9. D P K Y A Y F N G C S S P T A P L D P
10. P K Y A Y F N G C S S P T A P L D P
11. K Y A Y F N G C S S P T A P L D P
12. Y A Y F N G C S S P T A P L D P
13. A Y F N G C S S P T A P L D P
14. Y F N G C S S P T A P L D P
15. F N G C S S P T A P L D P
16. N G C S S P T A P L D P
17. G C S S P T A P L D P
18. C S S P T A P L D P
19. S S P T A P L D P
20. S P T A P L D P
21. P T A P L D P
22. A P L D P
23. P L D P
24. L D P
25. D P
26. P
27. .space

(12) D

1. P S K D C G D P K Y A Y F N G C S S P T A P L D P
2. P S K D C G S P K Y A Y F N G C S S P T A P L S P
3. P S K D C G A P K Y A Y F N G C S S P T A P L A P
4. P S K D C G D P K Y A Y F N G C S S P T A P L D
5. P S K D C G D P K Y A Y F N G C S S P T A P L
6. P S K D C G D P K Y A Y F N G C S S P T A P
7. P S K D C G D P K Y A Y F N G C S S P T A
8. P S K D C G D P K Y A Y F N G C S S P T
9. P S K D C G D P K Y A Y F N G C S S P
10. P S K D C G D P K Y A Y F N G C S S
11. P S K D C G D P K Y A Y F N G C S
12. P S K D C G D P K Y A Y F N G C
13. P S K D C G D P K Y A Y F N G
14. P S K D C G D P K Y A Y F N
15. P S K D C G D P K Y A Y F
16. P S K D C G D P K Y A Y
17. P S K D C G D P K Y A
18. P S K D C G D P K Y
19. P S K D C G D P K
20. P S K D C G D P
21. P S K D C G D
22. P S K D C G
23. P S K D C

24. P S K D
25. P S K
26. P S
27. P
28. .space
1.

(13) D

1. D P S K D C G D P K Y A Y F N G C S S P T A P L D P M D
2. S P S K D C G S P K Y A Y F N G C S S P T A P L S P M S
3. A P S K D C G A P K Y A Y F N G C S S P T A P L A P M A
4. P S K D C G D P K Y A Y F N G C S S P T A P L D P M D
5. S K D C G D P K Y A Y F N G C S S P T A P L D P M D
6. K D C G D P K Y A Y F N G C S S P T A P L D P M D
7. D C G D P K Y A Y F N G C S S P T A P L D P M D
8. C G D P K Y A Y F N G C S S P T A P L D P M D
9. G D P K Y A Y F N G C S S P T A P L D P M D
10. D P K Y A Y F N G C S S P T A P L D P M D
11. P K Y A Y F N G C S S P T A P L D P M D
12. K Y A Y F N G C S S P T A P L D P M D
13. Y A Y F N G C S S P T A P L D P M D
14. A Y F N G C S S P T A P L D P M D
15. Y F N G C S S P T A P L D P M D
16. F N G C S S P T A P L D P M D
17. N G C S S P T A P L D P M D
18. G C S S P T A P L D P M D
19. C S S P T A P L D P M D
20. S S P T A P L D P M D
21. S P T A P L D P M D
22. P T A P L D P M D
23. T A P L D P M D
24. A P L D P M D
25. P L D P M D
26. L D P M D
27. D P M D
28. P M D
29. M D
30. D
31. .space

(14) D

1. D P S K D C G D P K Y A Y F N G C S S P T A P L D P M D
2. S P S K D C G S P K Y A Y F N G C S S P T A P L S P M S
3. A P S K D C G A P K Y A Y F N G C S S P T A P L A P M A
4. D P S K D C G D P K Y A Y F N G C S S P T A P L D P M
5. D P S K D C G D P K Y A Y F N G C S S P T A P L D P
6. D P S K D C G D P K Y A Y F N G C S S P T A P L D
7. D P S K D C G D P K Y A Y F N G C S S P T A P L
8. D P S K D C G D P K Y A Y F N G C S S P T A P
9. D P S K D C G D P K Y A Y F N G C S S P T A
10. D P S K D C G D P K Y A Y F N G C S S P T
11. D P S K D C G D P K Y A Y F N G C S S P
12. D P S K D C G D P K Y A Y F N G C S S
13. D P S K D C G D P K Y A Y F N G C S
14. D P S K D C G D P K Y A Y F N G C
15. D P S K D C G D P K Y A Y F N G
16. D P S K D C G D P K Y A Y F N
17. D P S K D C G D P K Y A Y F
18. D P S K D C G D P K Y A Y
19. D P S K D C G D P K Y A
20. D P S K D C G D P K Y
21. D P S K D C G D P K
22. D P S K D C G D P
23. D P S K D C G D
24. D P S K D C G
25. D P S K D C
26. D P S K D
27. D P S K
28. D P S
29. D P
30. D
31. .space

(13) pS

1. pSPSKDCGpSPKYAYFNGCSSPT
2. pSPSKDCGpSPKYAYFNGCSSP
3. pSPSKDCGpSPKYAYFNGCSS
4. pSPSKDCGpSPKYAYFNGCS
5. pSPSKDCGpSPKYAYFNGC
6. pSPSKDCGpSPKYAYFNG
7. pSPSKDCGpSPKYAYFNG
8. pSPSKDCGpSPKYAYFN
9. pSPSKDCGpSPKYAYF
10. pSPSKDCGpSPKYAY
11. pSPSKDCGpSPKYA
12. pSPSKDCGpSPKY
13. pSPSKDCGpSPK
14. pSPSKDCGpSP
15. pSPSKDCGpS
16. pSPSKDCG
17. pSPSKDCGpSPKYAYFNG
18. PSKDCGpSPKYAYFNG
19. SKDCGpSPKYAYFNG
20. KDCGpSPKYAYFNG
21. DCGpSPKYAYFNG
22. CGpSPKYAYFNG
23. GpSPKYAYFNG
24. pSPKYAYFNG
25. PKYAYFNG
26. KYAYFNG
27. AYFNG
28. YFNG

(14)

1. dSPSKDCGdSPKYAYFNGCSSPT
2. dSPSKDCGdSPKYAYFNG
3. FNG
4. .space;

(13) D

1. A P L D P M D P P G Y K L V T G D R N N S S C R N
2. A P L S P M S P P G Y K L V T G D R N N S S C R N
3. A P L A P M A P P G Y K L V T G D R N N S S C R N
4. P L D P M D P P G Y K L V T G D R N N S S C R N
5. P L D P M D P P G Y K L V T G D R N N S S C R N
6. D P M D P P G Y K L V T G D R N N S S C R N
7. P M D P P G Y K L V T G D R N N S S C R N
8. M D P P G Y K L V T G D R N N S S C R N
9. D P P G Y K L V T G D R N N S S C R N
10. P P G Y K L V T G D R N N S S C R N
11. P G Y K L V T G D R N N S S C R N
12. G Y K L V T G D R N N S S C R N
13. Y K L V T G D R N N S S C R N
14. K L V T G D R N N S S C R N
15. L V T G D R N N S S C R N
16. V T G D R N N S S C R N
17. T G D R N N S S C R N
18. G D R N N S S C R N
19. R N N S S C R N
20. N N S S C R N
21. N S S C R N
22. S S C R N
23. S C R N
24. C R N
25. R N
26. N
27. .space

(14) D

2. A P L D P M D P P G Y K L V T G D R N N S S C R N
3. A P L S P M S P P G Y K L V T G D R N N S S C R N
4. A P L A P M A P P G Y K L V T G D R N N S S C R N
5. A P L D P M D P P G Y K L V T G D R N N S S C R
6. A P L D P M D P P G Y K L V T G D R N N S S C
7. A P L D P M D P P G Y K L V T G D R N N S S

8. A P L D P M D P P G Y K L V T G D R N N S
9. A P L D P M D P P G Y K L V T G D R N N
10. A P L D P M D P P G Y K L V T G D R N
11. A P L D P M D P P G Y K L V T G D R
12. A P L D P M D P P G Y K L V T G D
13. A P L D P M D P P G Y K L V T G
14. A P L D P M D P P G Y K L V T
15. A P L D P M D P P G Y K L V
16. A P L D P M D P P G Y K L
17. A P L D P M D P P G Y K
18. A P L D P M D P P G Y
19. A P L D P M D P P G
20. A P L D P M D P P
21. A P L D P M D P
22. A P L D P M D
23. A P L D P M
24. A P L D P
25. A P L D
26. A P L
27. A P
28. A

Figure 1: PDGF-β induces new intima in human saphenous veins in vitro, associated with an increase in Cx43 and proliferation markers

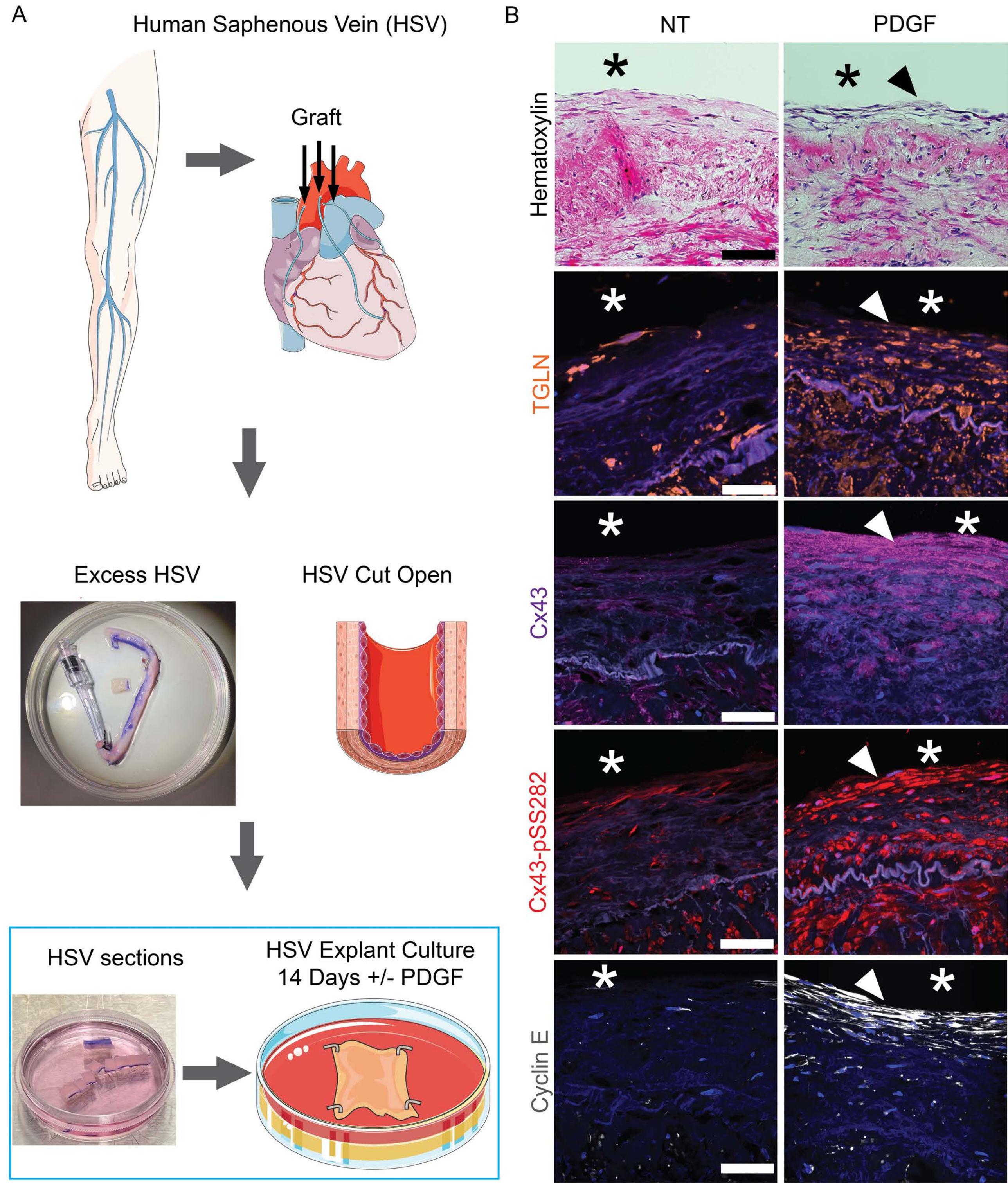

Figure 2: Design of the CycliCx peptide using peptide arrays demonstrates cyclin E binding regions on the phosphorylated Cx43CT

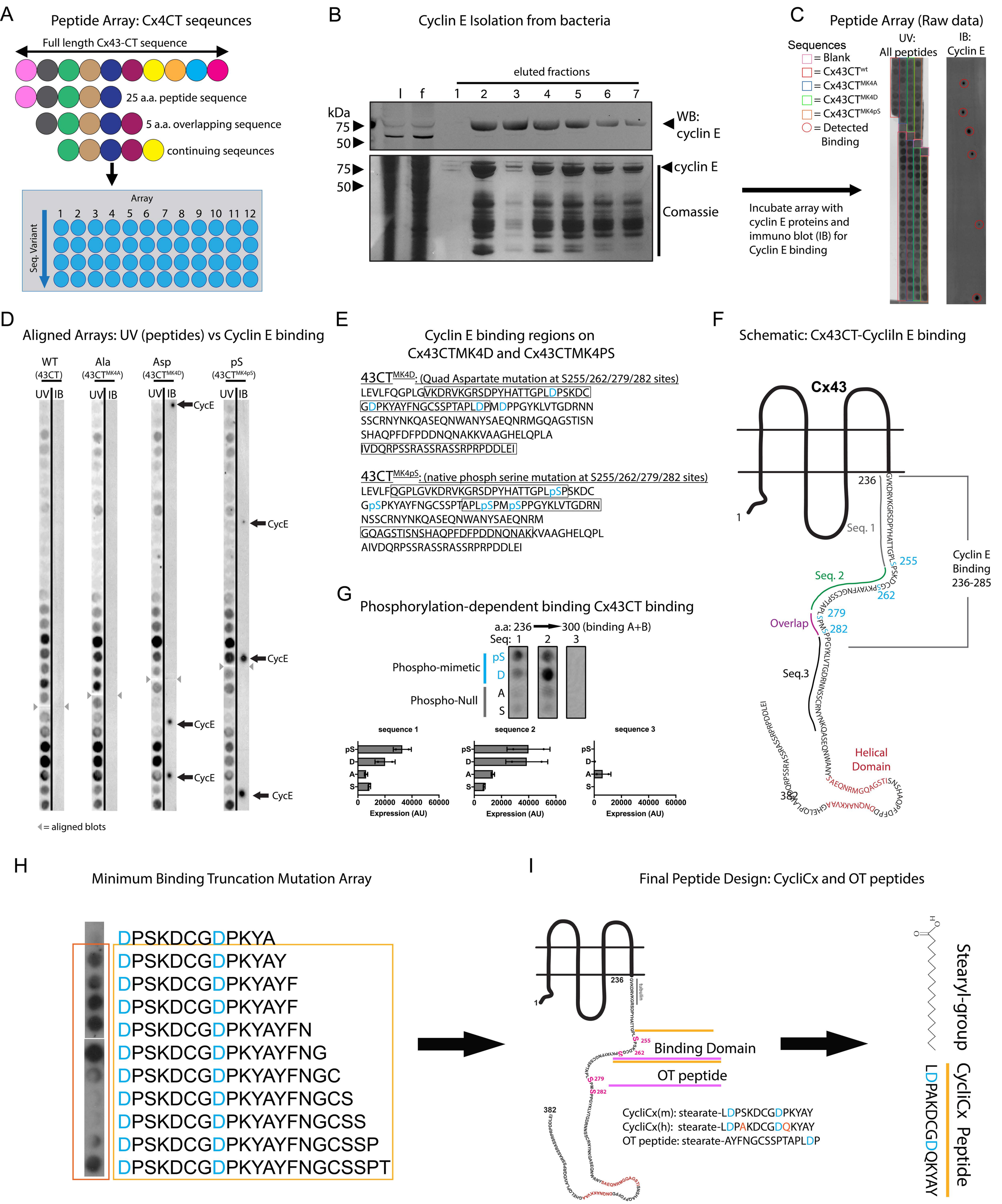

Figure 3: CycliCx Peptide alters Cx43 expression and interactions with cyclin E

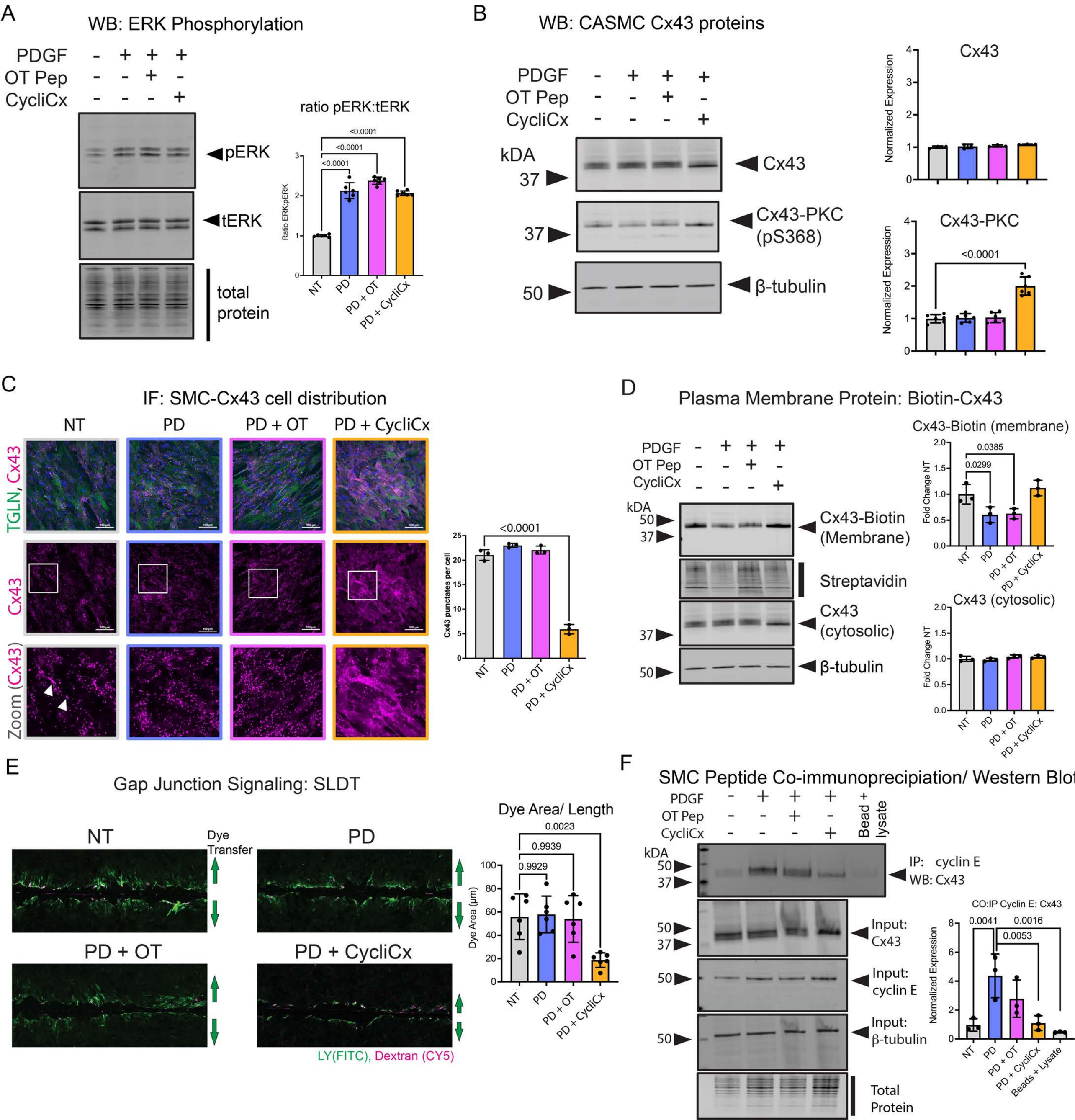

Figure 4: Transcriptomics reveals that the CycliCx peptide arrests cell cycle progression at G1/S phase transition

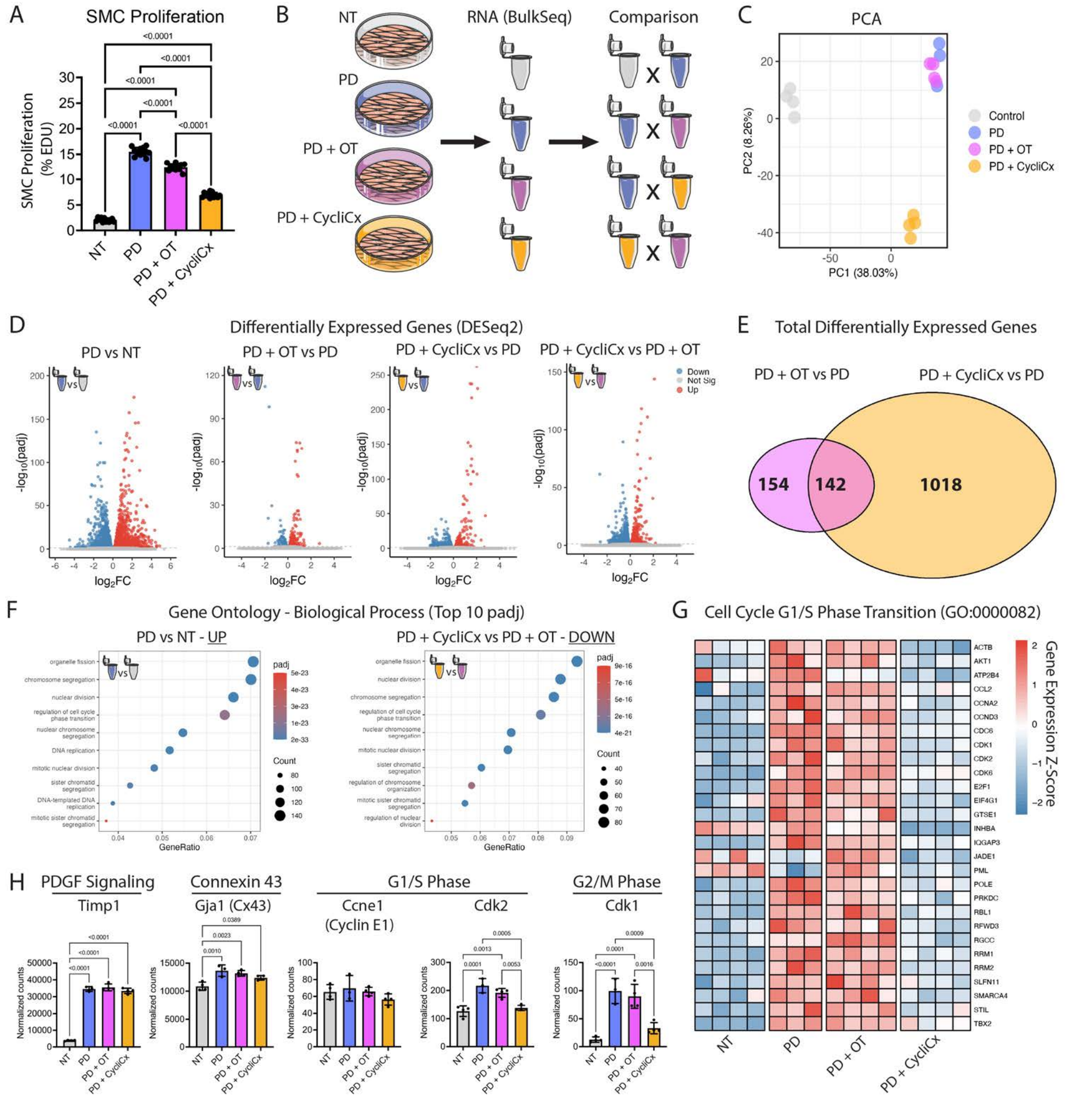
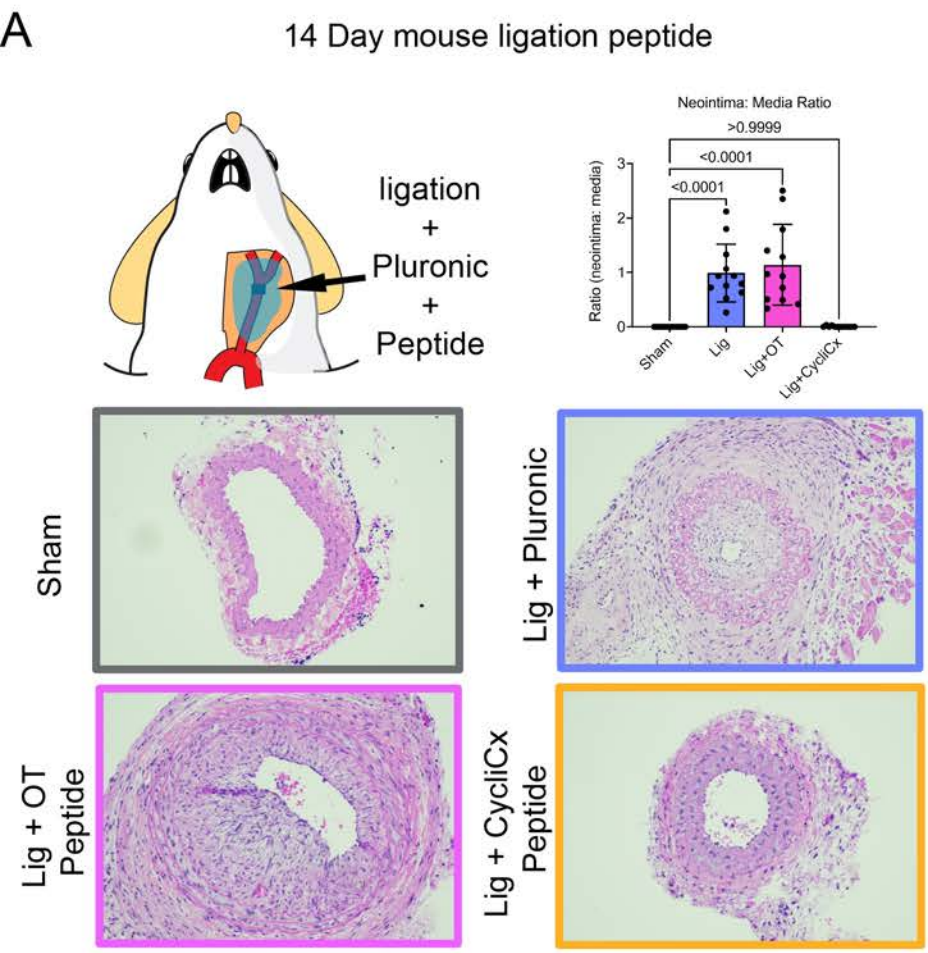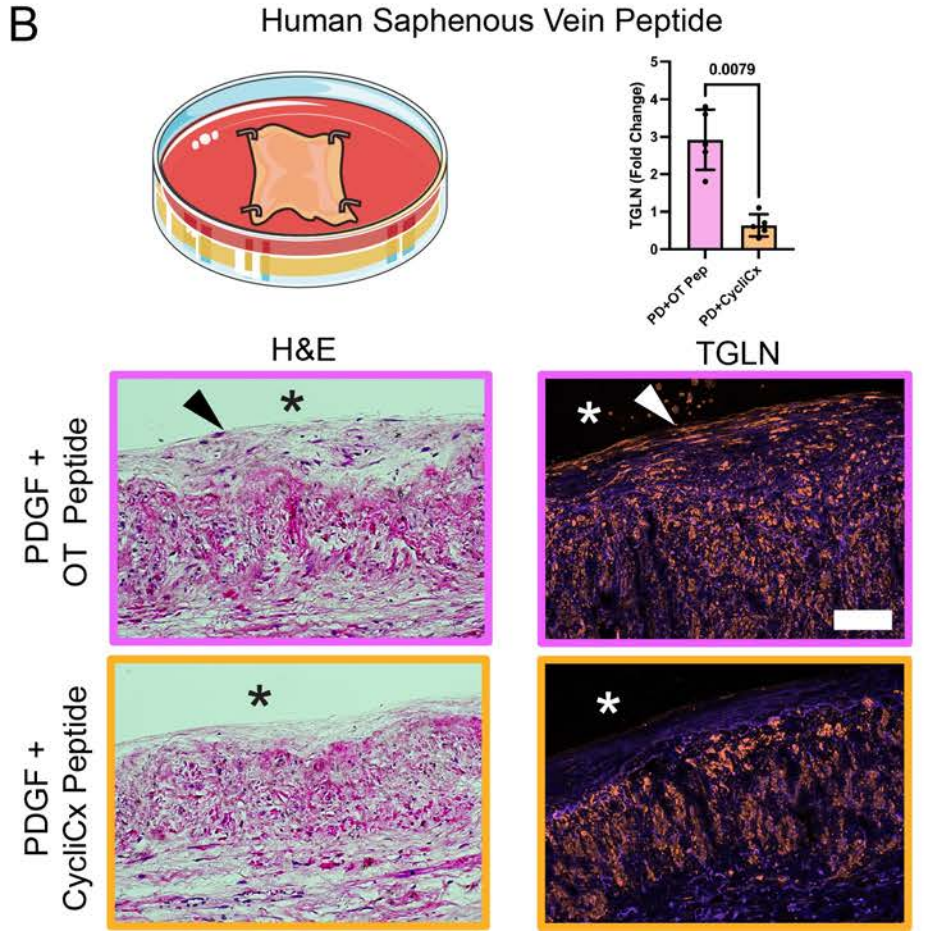
Figure 5: CycliCx peptide limits neointima formation in mouse and human blood vessels